

Spiro-centre substitution effects in intramolecular spin-spin interactions of spirobiacridine diradicals

Shinichi Ogawa, Takuya Kanetomo* and Masaya Enomoto*

Department of Chemistry, Faculty of Science Division 1,
Tokyo University of Science, 1-3 Kagurazaka, Shinjuku-ku, Tokyo, 162-8603, Japan

Table of Contents

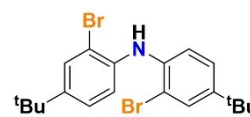
Materials and Methods	p. S2
Synthesis	pp. S3–S6
ESR	pp. S7–S8
Single-Crystal X-ray Diffractions	p. S9
Theoretical calculations	pp. S10–S31
Magnetic measurements	p. S32
¹ H and ¹³ C NMR spectra	pp. S33–S38
HRMS	pp. S39–S42
References	p. S43

Materials and Methods

Bis(4-*tert*-butylphenyl)amine was purchased from Tokyo Chemical Industry (TCI) Co., Ltd. Anhydrous *N,N'*-dimethylformamide (DMF) were used after distillation from a molecular sieve (4A). Dehydrated diethyl ether was purchased from KANTO Chemical Co., Inc. and used without further purification. ^1H and ^{13}C NMR experiments (400 and 100 MHz, respectively) were performed on an ECZ400S spectrometer (JEOL). The chemical shifts (given in ppm) were measured versus a reference peak of tetramethylsilane (TMS) in CDCl_3 and $\text{DMSO}-d_6$. The splitting patterns are designated as follows: s (singlet), d (doublet), t (triplet), dd (doublet of doublets), and m (multiplet). Infrared (IR) spectra were obtained on an FT/IR-4600 (JASCO) spectrometer using a diamond attenuated total reflectance (ATR) method. The spectral data are obtained as major peaks in wavenumbers (cm^{-1}) and recorded in a spectral window of 4000–400 cm^{-1} . Mass spectra (MS) were recorded in an electrospray ionization (ESI) mode using an AccuTOF-JMS-T100LP (JEOL) spectrometer. The specimen was dissolved in methanol. The experimental data was calibrated by YOKUDELNA. Electronic spectra (ultraviolet–visible, UV–Vis) were obtained on a JASCO V-650 spectrometer. Electron spin resonance (ESR) spectra were recorded on a Bruker ELEXSYS X-band (9.3 GHz) spectrometer. The ESR spectra were recorded at room temperature (RT) after the sample solution in toluene was thoroughly purged with the N_2 gas. Frozen solution ESR spectra were acquired after degassing with a freeze-thaw technique, and a cryostat (Oxford) was applied using liquid helium.

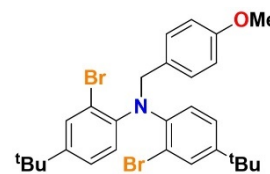
Synthesis

Synthesis of bis(2-bromo-4-*tert*-butylphenyl)amine (2). Compounds bis(4-*tert*-butylphenyl)amine (11.26 g, 40.01 mmol) and ammonium acetate (0.74 g, 9.6 mmol) were dissolved in chloroform (160 mL). *N*-Bromosuccinimide



(14.90 g, 83.7 mmol) as powder was added to the reaction mixture for 10 minutes at RT. The mixture underwent stirring for 1 h. The reaction was terminated by the addition of saturated Na₂S₂O₃ aqueous solution, followed by sequential washing with saturated NaHCO₃ aqueous solution and brine. The organic layer was dried over anhydrous MgSO₄, and the filtrate was concentrated under reduced pressure. The crude product purified by the recrystallization using ethanol, giving a pale yellow solid **2** (13.86 g, 31.55 mmol, 79%). Mp. 161–162 °C. ¹H NMR (400 MHz, CDCl₃, Fig. S16): δ 7.56 (d, *J* = 1.4 Hz, 2H), 7.21 (dd, *J* = 8.7 and 1.8 Hz, 4H), 6.26 (s, 1H) and 1.30 (s, 18H). ¹³C NMR (100 MHz, CDCl₃, Fig. S17): δ 145.68, 137.74, 130.03, 125.06, 117.58, 113.94, 34.28 and 31.32. HRMS (ESI+, Fig. S28): *m/z* calcd. for C₂₀H₂₆Br₂N [M+H]⁺: 440.04115, found: 440.04055. IR (ATR): 1517, 1497, 1331, 1258, 880, 812, 710, 600, 416 and 409 cm⁻¹. UV-Vis (chloroform) λ_{max}/nm (log ε) 290 (4.33).

Synthesis of *N*-(4-methoxybenzyl)-bis(2-bromo-4-*tert*-butylphenyl)amine (3). Compounds **2** (8.78 g, 20.0 mmol) and 60% NaH dispersion in paraffin liquid (1.20 g, 30 mmol) were stirred for 45 minutes in dried DMF solution (60 mL). After 4-methoxybenzyl chloride (4.1 mL,



30 mmol) was added, the reaction mixture was stirred overnight. The reaction was quenched with water, and then the colourless solid was collected. From the recrystallization using ethanol, the colourless solid **3** was a yield of 10.20 g (18.23 mmol, 91%). Mp. 177–178 °C (decomp). ¹H NMR (400 MHz, CDCl₃, Fig. S18): δ 7.54 (d, *J* = 2.3 Hz, 2H), 7.44 (d, *J* = 8.7 Hz, 2H), 7.13 (dd, *J* = 8.4 and 1.8 Hz, 2H), 6.85 (d, *J* = 8.2 Hz, 2H), 6.80 (d, *J* = 8.7 Hz, 2H), 4.70 (s, 2H), 3.75 (s, 3H) and 1.26 (s, 18H). ¹³C NMR (100 MHz, CDCl₃, Fig. S19): δ 158.4, 148.0, 144.5, 131.2, 130.2, 128.7, 124.7, 124.6, 120.9, 113.6, 56.2, 55.2, 34.3 and 31.2. HRMS (ESI+, Fig. S29): *m/z* calcd. for C₂₈H₃₃Br₂NONa [M+Na]⁺: 580.08266, found: 580.08221. IR (ATR): 1508, 1497, 1483, 1257, 1240, 1222, 1170, 824, 816 and 613 cm⁻¹. UV-Vis (chloroform) λ_{max}/nm (log ε) 283 (4.25).

Synthesis of 10,10'-bis(4-methoxybenzyl)-2,2',7,7'-tetra(*tert*-butyl)-9,9'-(10*H*,10'*H*)-spirobisilacridine (4-Si). Compound **3** (3.92 g, 7.01 mmol) was dissolved in anhydrous diethyl ether (70 mL) under an Ar atmosphere. The solution was stirred for 1 h at –80 °C. After *n*-BuLi in *n*-hexane (1.57 mol L⁻¹, 9.8 mL, 15.4 mmol) was added, the mixture was

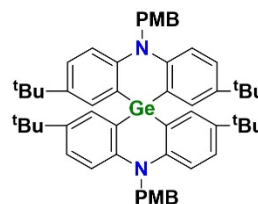


stirred for 15 minutes. The solution was stirred for 2 h at RT and then for 1 h at ice bath. Tetrachlorosilane (0.41 mL, 3.6 mmol) was added, the mixture was 15 minutes at ice bath and then

for 30 minutes at RT. The reaction mixture was refluxed overnight. The reaction was quenched with saturated NH₄Cl aqueous solution. The collected solid was washed with water and diethyl ether to give the colourless solid **4-Si** (1.90 g, 2.30 mmol, 66%). Mp. > 300 °C. ¹H NMR (400 MHz, CDCl₃, Fig. S20): δ 7.40 (d, *J* = 1.8 Hz, 4H), 7.29 (m, 8H), 6.95 (m, 8H), 5.29 (s, 4H), 3.83 (s, 6H) and 1.18 (s, 36H). ¹³C NMR (100 MHz, CDCl₃, Fig. S21): δ 158.47, 148.66, 142.22, 131.64, 130.46, 127.63, 127.43, 119.04, 115.48, 114.20, 55.49, 55.32, 33.96 and 31.36. HRMS (ESI+, Fig. S30): *m/z* calcd. for C₅₆H₆₆N₂NaO₂Si [M+Na]⁺: 849.47912, found: 849.48270. IR (ATR): 1510, 1458, 1451, 1398, 1240, 1223, 820, 565, 497 and 457 cm⁻¹. UV-Vis (chloroform) λ_{max}/nm (log ε) 286 (4.58).

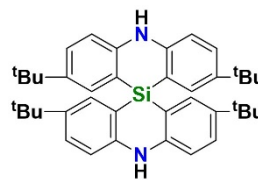
Synthesis of 10,10'-bis(4-methoxybenzyl)-2,2',7,7'-tetra(*tert*-butyl)-9,9'(10*H*,10'*H*)-spirobigermaacridine (4-Ge).

Compound **3** (5.22 g, 9.33 mmol) was dissolved in anhydrous diethyl ether (50 mL) under the Ar atmosphere. The solution was stirred for 1 h at -80 °C. After *n*-BuLi in *n*-hexane (1.56 mol L⁻¹, 13.2 mL, 20.6 mmol) was added, the mixture was stirred for 15 minutes. The solution was stirred for 2 h at RT and then for 1 h at ice bath. Tetrachlorogermane (1.0 g, 4.7 mmol) was added, the mixture was 15 minutes at ice bath and then for 30 minutes at RT. The reaction mixture was refluxed overnight. The reaction was quenched with saturated NH₄Cl aqueous solution. The collected solid was washed with water and diethyl ether to give the colourless solid **4-Ge** (2.77 g, 3.18 mmol, 68%). Mp. > 300 °C. ¹H NMR (400 MHz, CDCl₃, Fig. S22): δ 7.37 (d, *J* = 2.3 Hz, 4H), 7.32 (d, *J* = 8.2 Hz, 4H), 7.23 (dd, *J* = 8.7 and 2.7 Hz, 4H), 7.01 (d, *J* = 8.7 Hz, 4H), 6.91 (d, *J* = 8.7 Hz, 4H), 5.24 (s, 4H), 3.82 (s, 6H) and 1.19 (s, 36H). ¹³C NMR (100 MHz, CDCl₃, Fig. S23): δ 158.37, 148.54, 142.99, 131.13, 130.66, 127.66, 126.96, 121.97, 116.39, 114.11, 56.09, 55.30, 34.01 and 31.34. HRMS (ESI+, Fig. S31): *m/z* calcd. for C₅₆H₆₆GeN₂NaO₂ [M+Na]⁺: 895.42338, found: 895.42003. IR (ATR): 1510, 1453, 1396, 1241, 1221, 1199, 1170, 1038, 820 and 445 cm⁻¹. UV-Vis (chloroform) λ_{max}/nm (log ε) 297 (4.38).



Synthesis of 2,2',7,7'-tetra(*tert*-butyl)-9,9'(10*H*, 10'*H*)-spirobisilaacridine (5-Si).

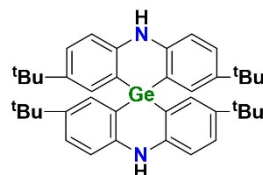
Compounds **4-Si** (827 mg, 1.00 mmol) and 90% 2,3-dichloro-5,6-dicyano-1,4-benzoquinone (DDQ, 555 mg, 2.20 mmol) were dissolved in toluene (10 mL). The mixture was stirred overnight at 40 °C. After the cooling to RT, the reaction was quenched with saturated NaHCO₃ aqueous solution. The organic layer was extracted by chloroform and washed with brine. The solution was dried over anhydrous MgSO₄, and thus the filtrate was concentrated under reduced pressure. The black oil was purified by silica-gel column chromatography eluted with 2/3 chloroform/*n*-hexane, to afford a yellow solid **5-Si** (54.4 mg, 0.0927 mmol, 9%). Mp. 142–143 °C. ¹H NMR (400 MHz, DMSO-*d*₆, Fig. S24): δ 9.21 (s, 2H), 7.35 (dd, *J* = 8.7 and 2.3 Hz, 4H), 7.06 (d, *J* = 8.7 Hz, 4H), 7.03 (d, *J* = 2.3 Hz, 4H) and



1.09 (s, 36H). ^{13}C NMR (100 MHz, CDCl_3 , Fig. S25): δ 145.08, 141.82, 132.68, 127.71, 115.05, 114.45, 34.01 and 31.40. HRMS (ESI+, Fig. S32): m/z calcd. for $\text{C}_{40}\text{H}_{50}\text{N}_2\text{Si}$ $[\text{M}]^+$: 586.37432, found: 586.37190. IR (ATR): 1601, 1456, 1359, 1237, 1120, 1083, 811, 523, 491 and 462 cm^{-1} . UV-Vis (chloroform) $\lambda_{\text{max}}/\text{nm}$ ($\log \epsilon$) 285 (4.43).

Synthesis of 2,2',7,7'-tetra(*tert*-butyl)-9,9'(10*H*,10'*H*)-

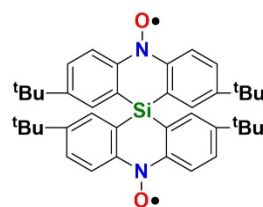
spirobigermaacridine (5-Ge). Compounds **4-Ge** (436 mg, 0.50 mmol) and 90% DDQ (278 mg, 1.10 mmol) were dissolved in toluene (5 mL). The mixture was stirred overnight at $40\text{ }^\circ\text{C}$. After the cooling to RT, the reaction



was quenched with saturated NaHCO_3 aqueous solution. The organic layer was extracted by chloroform and washed with brine. The solution was dried over anhydrous MgSO_4 , and thus the filtrate was concentrated under reduced pressure. The brown oil was purified by silica-gel column chromatography eluted with 2/1 chloroform/*n*-hexane, to afford a yellow solid **5-Ge** (115.7 mg, 0.183 mmol, 37%). Mp. $170\text{--}171\text{ }^\circ\text{C}$. ^1H NMR (400 MHz, $\text{DMSO-}d_6$, Fig. S26): δ 8.96 (s, 2H), 7.31 (dd, $J = 8.7$ and 2.5 Hz, 4H), 7.04 (d, $J = 8.6$ Hz, 2H), 7.00 (d, $J = 2.5$ Hz, 2H) and 1.10 (s, 36H). ^{13}C NMR (100 MHz, CDCl_3 , Fig. S27): δ 144.74, 142.36, 132.14, 127.18, 116.91, 114.75, 34.04 and 31.41. HRMS (ESI+, Fig. S33): m/z calcd. for $\text{C}_{40}\text{H}_{50}\text{GeN}_2\text{Na}$ $[\text{M}+\text{Na}]^+$: 655.30835, found: 655.30789. IR (ATR): 2953, 1598, 1461, 1389, 1359, 1320, 1271, 1234, 809 and 446 cm^{-1} . UV-Vis (chloroform) $\lambda_{\text{max}}/\text{nm}$ ($\log \epsilon$) 288 (4.31).

Synthesis of 2,2',7,7'-tetra(*tert*-butyl)-9,9'(10*H*,10'*H*)-

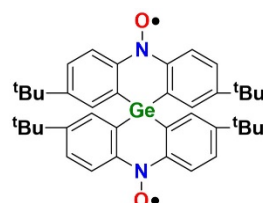
spirobisilaacridine-10,10'-dioxyl (1-Si). Compound **5-Si** (54.4 mg, 0.093 mmol) was dissolved in chloroform (3 mL). The 65% *m*-chloroperbenzoic acid (*m*-CPBA, 152.0 mg, 0.573 mmol) dissolved in chloroform (7.5 mL) was added to at $0\text{ }^\circ\text{C}$, and the mixture was stirred for 4 h. The mixture was



passed through the short column (activated aluminum, eluted with chloroform), and the filtrate was concentrated under reduced pressure. The brown solid was purified by silica-gel column chromatography eluted with 1/9 ethyl acetate/*n*-hexane, to afford dark brown solid. Recrystallization from CH_2Cl_2 and *n*-hexane in a refrigerator gave dark red platelet crystals **1-Si** (6.8 mg, 0.011 mmol, 12%), which were subjected to analytical, structural and magnetic studies. Mp. $208\text{--}209\text{ }^\circ\text{C}$. HRMS (ESI+, Fig. S34): m/z calcd. for $\text{C}_{40}\text{H}_{48}\text{N}_2\text{NaO}_2\text{Si}$ $[\text{M}+\text{Na}]^+$: 639.33827, found: 639.33911. IR (ATR): 1388, 1350, 1261, 1127, 1119, 831, 775, 529, 502 and 446 cm^{-1} . UV-Vis (chloroform) $\lambda_{\text{max}}/\text{nm}$ ($\log \epsilon$) 347 (4.50).

Synthesis of 2,2',7,7'-tetra(*tert*-butyl)-9,9'(10*H*,10'*H*)-

spirobigermaacridine-10,10'-dioxyl (1-Ge). Compound **5-Ge** (61.1 mg,



0.097 mmol) was dissolved in chloroform (3 mL). The 65% *m*-CPBA (154.1 mg, 0.580 mmol) dissolved in chloroform (7.5 mL) was added to at 0 °C, and the mixture was stirred for 3 h. The mixture was passed through the short column (activated aluminum, eluted with chloroform), and the filtrate was concentrated under reduced pressure. The brown solid was purified by silica-gel column chromatography eluted with 1/9 ethyl acetate/*n*-hexane, to afford dark brown solid. Recrystallization from CH₂Cl₂ and *n*-hexane in a refrigerator gave dark red platelet crystals **1-Ge** (11.5 mg, 0.017 mmol, 18%), which were subjected to analytical, structural and magnetic studies. Mp. 217–218 °C. HRMS (ESI+, Fig. S35): *m/z* calcd. for C₄₀H₄₈GeN₂NaO₂ [M+Na]⁺: 685.28253, found: 685.28575. IR (ATR): 2958, 1449, 1388, 1345, 1260, 1119, 828, 513, 448 and 439 cm⁻¹. UV-Vis (chloroform) λ_{max}/nm (log ε) 341 (4.67).

ESR Studies

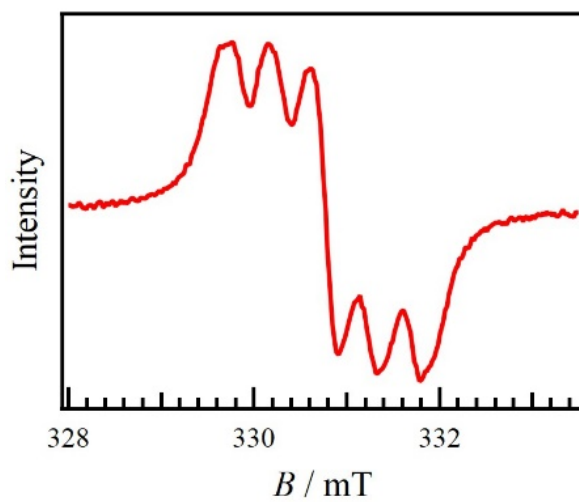


Fig. S1. X-Band ESR spectrum for **1-Si** in a degassed toluene solution at RT.

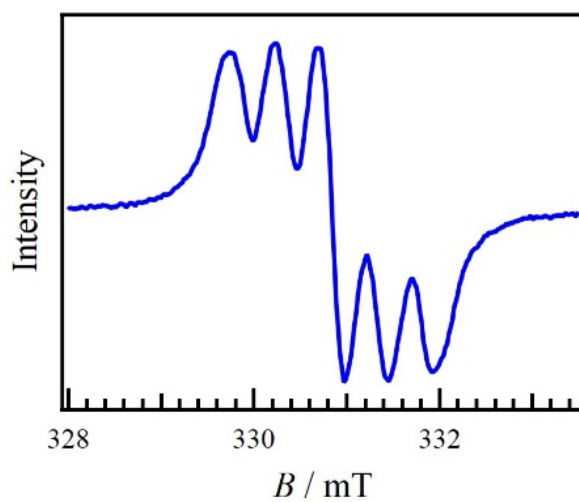


Fig. S2. X-Band ESR spectrum for **1-Ge** in a degassed toluene solution at RT.

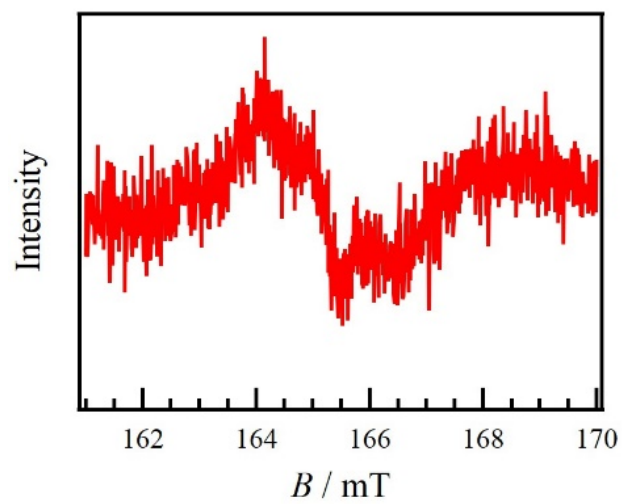


Fig. S3. Frozen-solution X-band ESR spectrum for **1-Si** in the degassed toluene solution at 40 K.

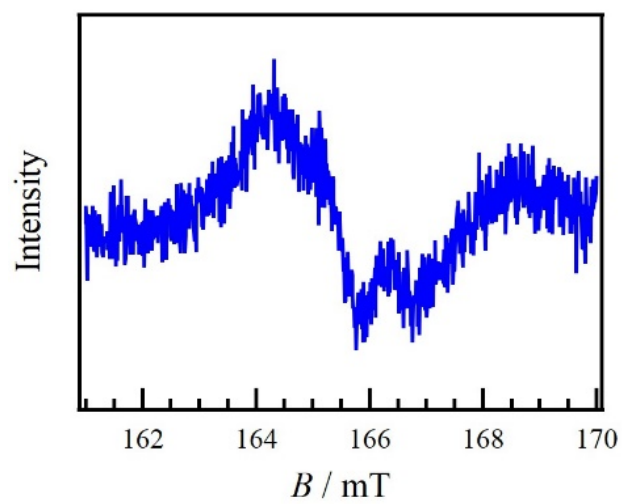


Fig. S4. Frozen-solution X-band ESR spectrum for **1-Ge** in the degassed toluene solution at 50 K.

Single Crystal X-ray Diffractions

The X-ray diffraction data of **1-Si** and **1-Ge** at 93 K were collected on a Rigaku VariMax Dual (Mo K α radiation: $\lambda = 0.71073$ Å). The selected crystallographic data are given in Table S1. X-ray data analyses were carried out using the SHELXT^{S1} and SHELXL^{S2} programs operated with the Olex2 interface.^{S3} All the hydrogen atoms were refined as “riding”. The thermal displacement parameters of the non-hydrogen atoms were refined anisotropically. The CCDC numbers of **1-Si** and **1-Ge** are 2334921 and 2334922, respectively.

Table S1. Selected crystallographic data for **1-Si** and **1-Ge** (**1-C** as the reference).

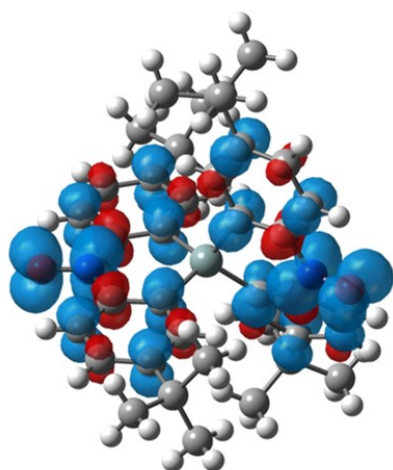
	1-Si	1-Ge	1-C ^a
Formula	C ₈₀ H ₉₆ N ₄ O ₂ Si ₂	C ₄₀ H ₄₈ GeN ₂ O ₂	C ₄₁ H ₄₈ N ₂ O ₂
Fw	1233.78	661.39	600.84
T/K	93	93	100
Crystal system	Triclinic	Monoclinic	Monoclinic
Space group	<i>P</i> -1	<i>P</i> 2 ₁ / <i>n</i>	<i>P</i> 2 ₁ / <i>n</i>
<i>a</i> /Å	11.26630(10)	12.3869(3)	10.794(2)
<i>b</i> /Å	17.6483(2)	25.3893(5)	19.316(4)
<i>c</i> /Å	18.7120(3)	11.2881(3)	16.518(3)
α /°	90.8560(10)	90	90
β /°	96.450(10)	105.385(3)	90.760(11)
γ /°	107.5730(10)	90	90
<i>V</i> /Å ³	3519.75(8)	3422.83(15)	3443.6(12)
<i>Z</i>	2	4	4
<i>d</i> _{calcd} /g cm ⁻³	1.164	1.283	1.159
μ /Mo K α /mm ⁻¹	0.103	0.932	0.070
<i>R</i> (<i>F</i>) ^a (<i>I</i> > 2 σ (<i>I</i>))	0.0371	0.0308	0.0478
<i>R</i> _w (<i>F</i> ²) ^b (all data)	0.1024	0.0834	0.1182
Goodness of fit	1.035	1.037	1.069

^a Ref. [S4]. ^b $R = \sum ||F_o| - |F_c|| / \sum |F_o|$. ^c $R_w = [\sum w|F_o^2 - F_c^2|^2 / \sum w(F_o^2)^2]^{1/2}$.

Theoretical calculations

The DFT calculations of **1-Si-a**, **1-Si-b** and **1-Ge** were performed on the Gaussian09 program.^{S5} The energies of the triplet (T) and broken-symmetry singlet (BS) states were calculated at the UB3LYP/6-311G+(2d,p) level. The structural parameters were given from the crystallographic data. The calculated spin densities of the T and BS states for **1-Si-a**, **1-Si-b** and **1-Ge** have been mapped onto the molecular skeleton shown in Figs. S5–S7, respectively. The triplet and singlet energy states for **1-Si-a**, **1-Si-b** and **1-Ge** are summarized in Tables S2–S4, respectively. Selected molecular orbitals of the ground triplet state ($S = 1$) and α and β spins for **1-Si-a**, **1-Si-b** and **1-Ge** with isovalue = 0.03 are shown in Tables S5–S7, respectively.

a)



b)

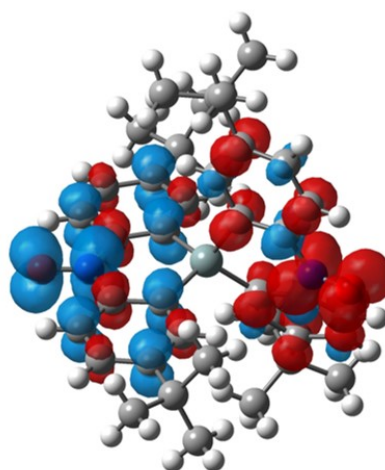
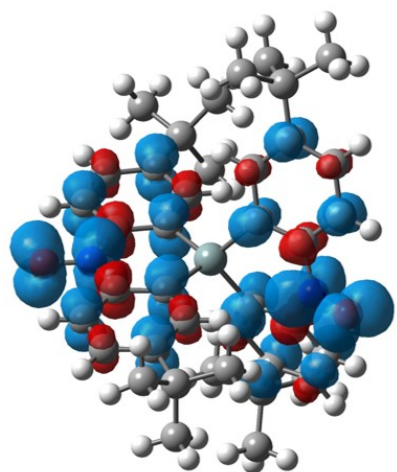


Fig. S5. Spin density maps drawn from the DFT MO calculations for **1-Si-a** with the (a) triplet and (b) singlet states. Blue and red lobes stand for positive and negative spin densities, respectively, with the isocontour of $0.002 e \text{ \AA}^{-3}$.

a)



b)

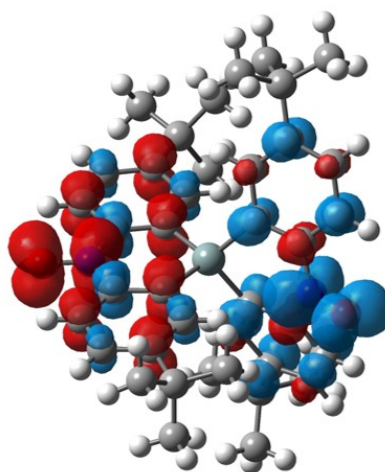
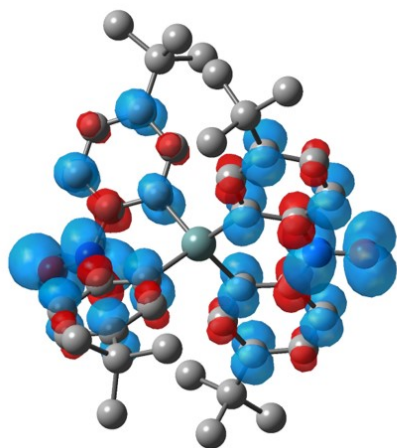


Fig. S6. Spin density maps drawn from the DFT MO calculations for **1-Si-b** with the (a) triplet and (b) singlet states. Blue and red lobes stand for positive and negative spin densities, respectively, with the isocontour of $0.002 e \text{ \AA}^{-3}$.

a)



b)

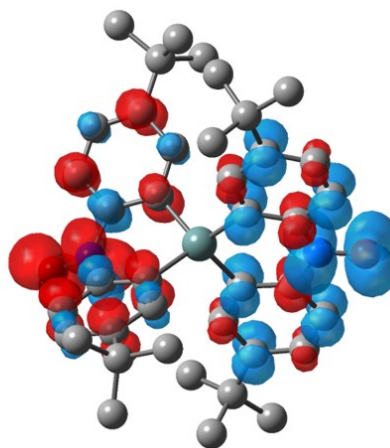


Fig. S7. Spin density maps drawn from the DFT MO calculations for **1-Ge** with the (a) triplet and (b) singlet states. Blue and red lobes stand for positive and negative spin densities, respectively, with the isocontour of $0.002 e \text{ \AA}^{-3}$.

Table S2. The energy levels and $\langle S^2 \rangle$ in the triplet and singlet spin states for **1-Si-a**.

Spin states	E / au	$\langle S^2 \rangle$
$S = 1$ (triplet)	-2102.59121432	2.0005
$S = 0$ (singlet)	-2102.59117798	0.2263

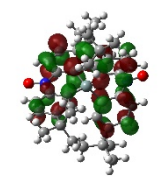
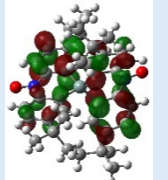
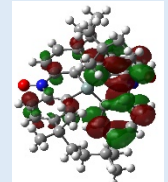
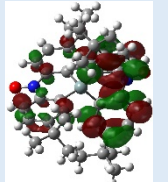
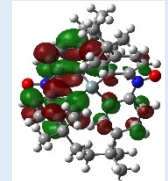
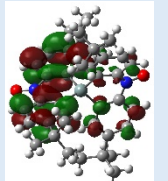
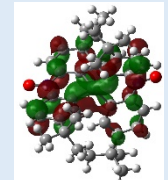
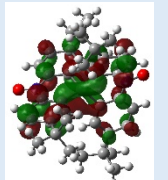
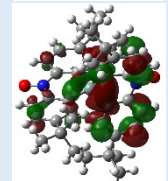
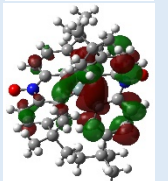
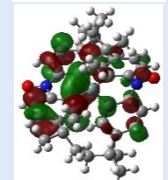
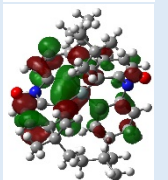
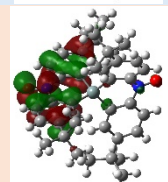
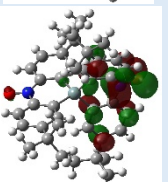
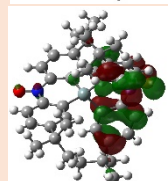
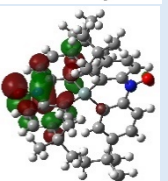
Table S3. The energy levels and $\langle S^2 \rangle$ in the triplet and singlet spin states for **1-Si-b**.

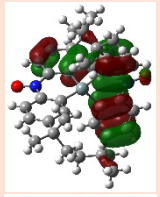
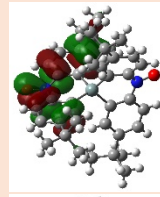
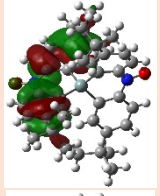
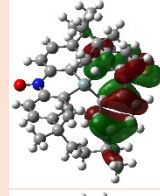
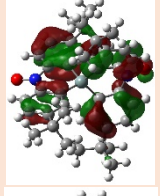
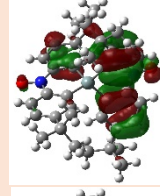
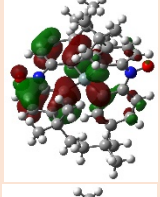
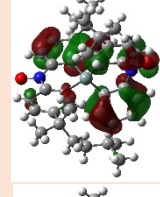
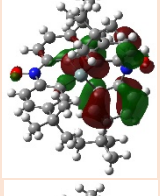
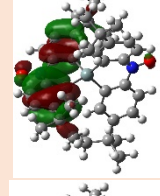
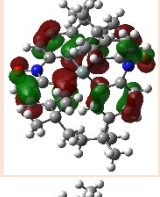
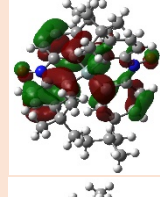
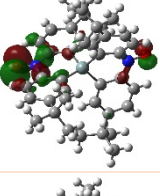
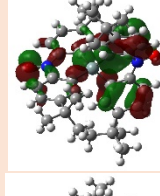
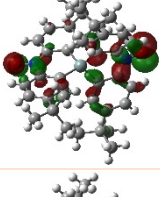
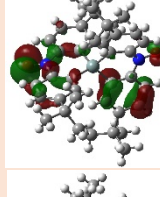
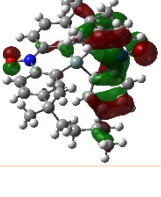
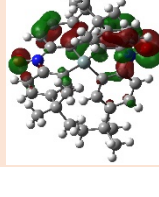
Spin states	E / au	$\langle S^2 \rangle$
$S = 1$ (triplet)	-2102.59975232	2.0005
$S = 0$ (singlet)	-2102.59972061	0.2210

Table S4. The energy levels and $\langle S^2 \rangle$ in the triplet and singlet spin states for **1-Ge**.

Spin states	E / au	$\langle S^2 \rangle$
$S = 1$ (triplet)	-3889.84438544	2.0005
$S = 0$ (singlet)	-3889.84434641	0.2170

Table S5. Selected molecular orbitals of the triplet state ($S = 1$) and α and β spins for **1-Si-a** (isovalue = 0.03). Red and blue filled cells represent the occupied and unoccupied MOs, respectively.

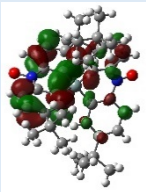
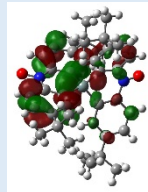
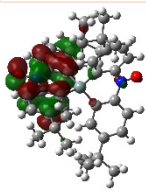
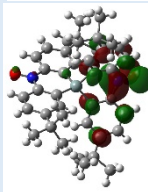
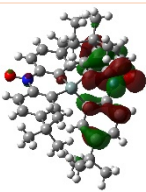
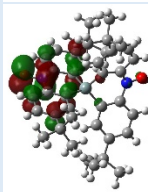
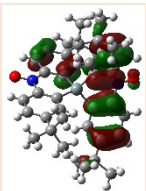
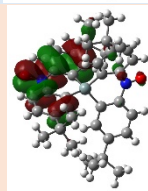
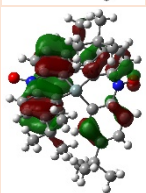
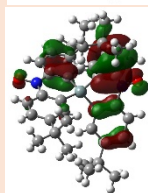
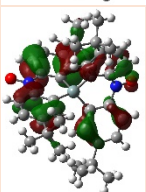
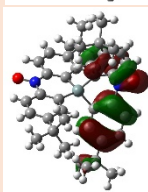
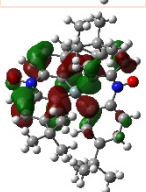
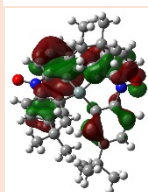
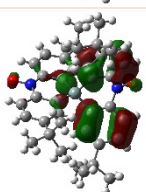
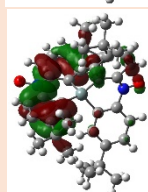
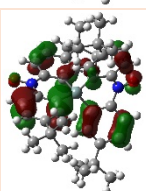
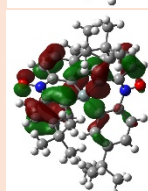
MOs (α spin)	E / eV		MOs (β spin)	E / eV	
173	-0.379		173	-0.251	
172	-0.478		172	-0.391	
171	-0.546		171	-0.444	
170	-0.985		170	-0.909	
169	-1.148		169	-1.091	
168	-1.261		168	-1.197	
167	-5.215 (SOMO)		167	-2.727	
166	-5.270 (SOMO)		166	-2.769	

165	-6.877		165	-6.640	
164	-6.993		164	-6.767	
163	-7.005		163	-6.819	
162	-7.143		162	-6.906	
161	-7.201		161	-6.939	
160	-7.454		160	-7.164	
159	-7.537		159	-7.166	
158	-7.608		158	-7.267	
157	-7.683		157	-7.319	

156	-7.706		156	-7.437	
-----	--------	--	-----	--------	--

Table S6. Selected molecular orbitals of the triplet state ($S = 1$) and α and β spins for **1-Si-b** (isovalue = 0.03). Red and blue filled cells represent the occupied and unoccupied MOs, respectively.

MOs (α spin)	E / eV		MOs (β spin)	E / eV	
175	-0.093		175	0.025	
174	-0.217		174	-0.215	
173	-0.377		173	-0.258	
172	-0.464		172	-0.374	
171	-0.524		171	-0.418	
170	-0.976		170	-0.898	
169	-1.140		169	-1.084	

168	-1.269		168	-1.204	
167	-5.223 (SOMO)		167	-2.712	
166	-5.299 (SOMO)		166	-2.780	
165	-6.826		165	-6.663	
164	-6.990		164	-6.756	
163	-7.029		163	-6.809	
162	-7.144		162	-6.905	
161	-7.233		161	-6.957	
160	-7.431		160	-7.152	

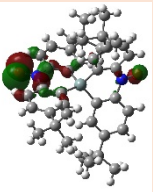
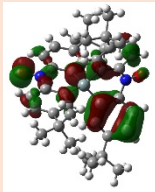
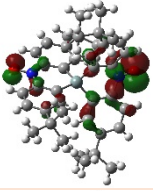
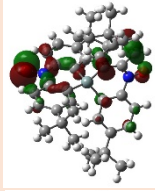
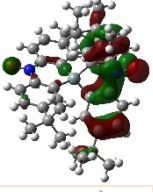
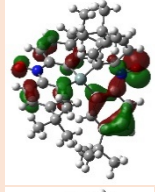
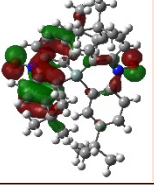
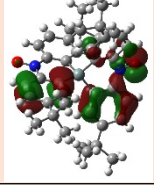
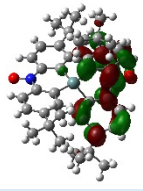
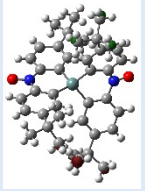
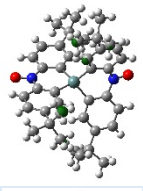
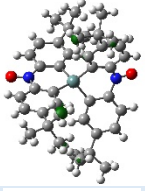
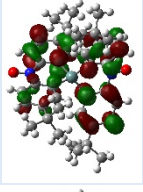
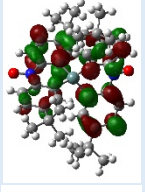
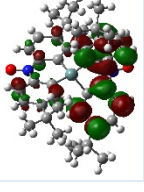
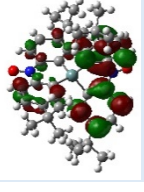
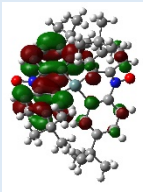
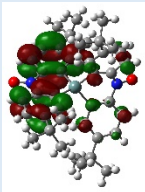
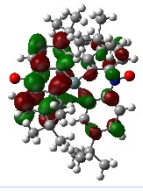
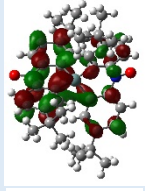
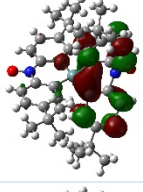
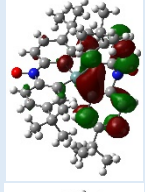
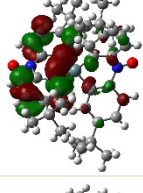
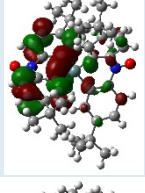
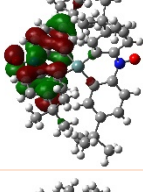
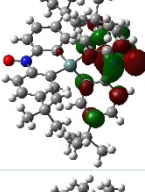
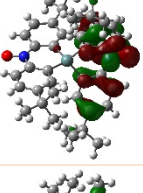
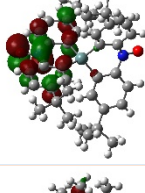
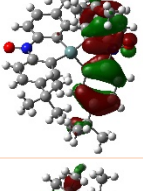
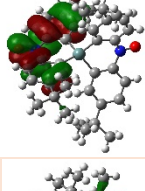
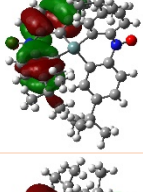
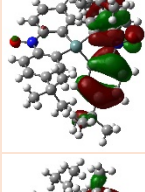
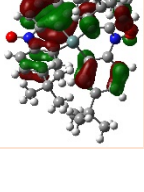
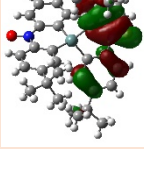
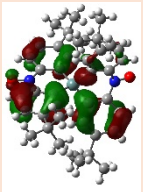
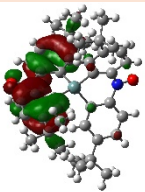
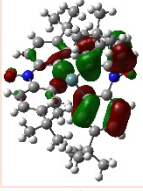
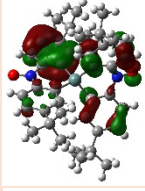
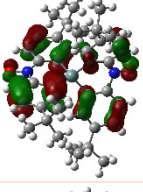
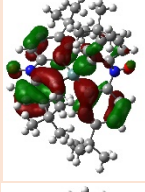
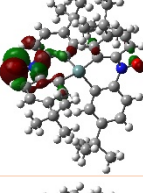
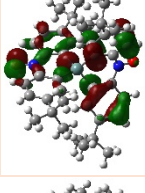
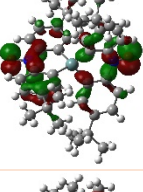
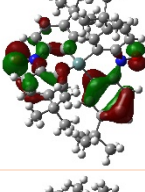
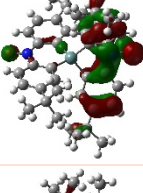
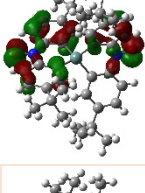
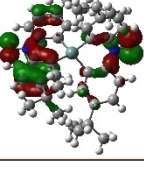
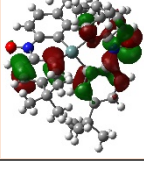
159	-7.544		159	-7.188	
158	-7.612		158	-7.282	
157	-7.680		157	-7.306	
156	-7.707		156	-7.422	

Table S7. Selected molecular orbitals of the triplet state ($S = 1$) and α and β spins for **1-Ge** (isovalue = 0.03). Red and blue filled cells represent the occupied and unoccupied MOs, respectively.

MOs (α spin)	E / eV		MOs (β spin)	E / eV	
184	-0.145		184	0.003	
183	-0.236		183	-0.233	
182	-0.405		182	-0.295	
181	-0.446		181	-0.365	

180	-0.548		180	-0.450	
179	-0.845		179	-0.759	
178	-1.068		178	-1.015	
177	-1.127		177	-1.061	
176	-5.185 (SOMO)		176	-2.643	
175	-5.295 (SOMO)		175	-2.747	
174	-6.847		174	-6.617	
173	-6.988		173	-6.764	
172	-7.049		172	-6.820	

171	-7.072		171	-6.927	
170	-7.194		170	-6.963	
169	-7.383		169	-7.079	
168	-7.511		168	-7.130	
167	-7.574		167	-7.240	
166	-7.647		166	-7.275	
165	-7.685		165	-7.422	

Compounds 9,9'(10*H*,10'*H*)spirobisilaacridine-10,10'-dioxyl (**SBDO-Si**) and 9,9'(10*H*,10'*H*)spirobigermaacridine-10,10'-dioxyl (**SBDO-Ge**), as model compounds to **1-Si** and **1-Ge**, and 9,9'(10*H*,10'*H*)spirobiacridine-10,10'-dioxyl (**SBDO-C**) were subjected to DFT calculations at the UB3LYP/6-311g+(2d,p) level, after the geometry was optimized at the UB3LYP/6-31g(d,p) level. The calculated spin densities of the T and BS states have been mapped onto the molecular skeleton shown in Figs. S8–S10. The triplet and singlet energy states for **SBDO-C**, **-Si** and **-Ge** are summarized in Tables S8–10, respectively. Selected molecular orbitals of the triplet state ($S = 1$) and α and β spins for **SBDO-C**, **-Si** and **-Ge** (isovalue = 0.03) are shown in Tables S11–S13.

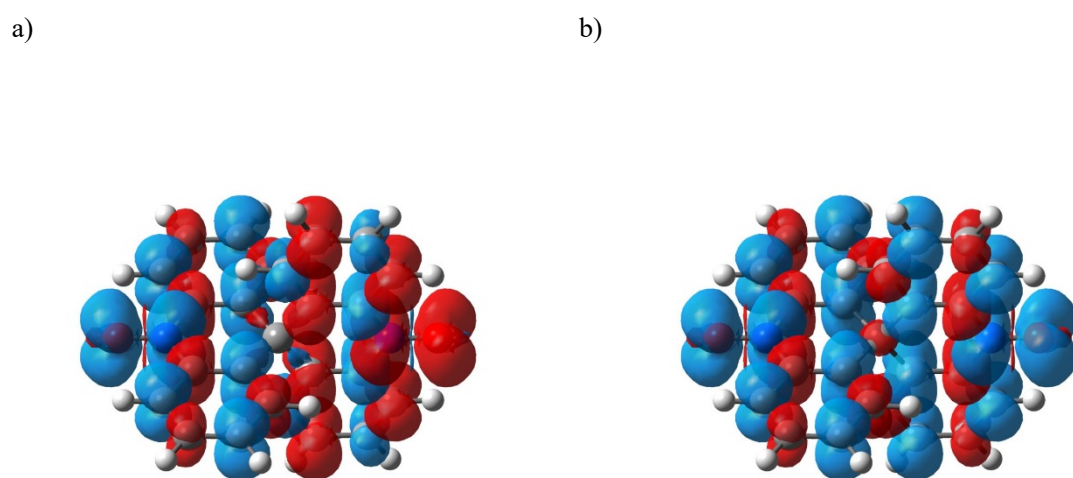
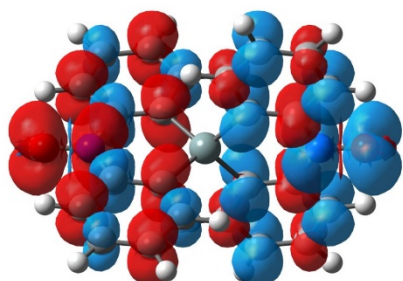


Fig. S8. Spin density maps drawn from the DFT MO calculations for **SBDO-C** with the (a) singlet and (b) triplet states. Blue and red lobes stand for positive and negative spin densities, respectively, with the isocontour of $0.001 \text{ e } \text{\AA}^{-3}$.

a)



b)

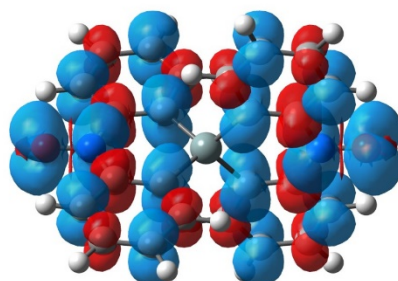
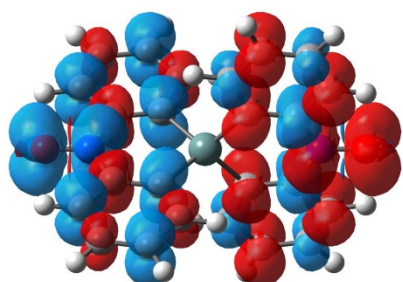


Fig. S9. Spin density maps drawn from the DFT MO calculations for **SBDO-Si** with the (a) singlet and (b) triplet states. Blue and red lobes stand for positive and negative spin densities, respectively, with the isocontour of $0.001 \text{ e } \text{\AA}^{-3}$.

a)



b)

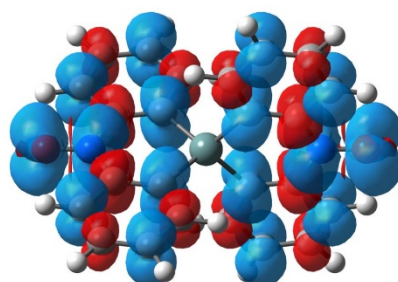


Fig. S10. Spin density maps drawn from the DFT MO calculations for **SBDO-Ge** with the (a) singlet and (b) triplet states. Blue and red lobes stand for positive and negative spin densities, respectively, with the isocontour of $0.001 \text{ e } \text{\AA}^{-3}$.

Table S8. The energy levels and $\langle S^2 \rangle$ in the triplet and singlet spin states for **SBDO-C**.

Spin states	E / au	$\langle S^2 \rangle$
$S = 1$ (triplet)	-1222.48767313	2.0007
$S = 0$ (singlet)	-1222.48758900	0.2523

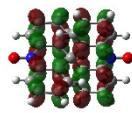
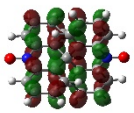
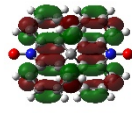
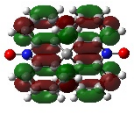
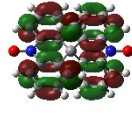
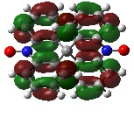
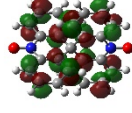
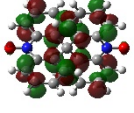
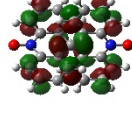
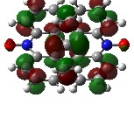
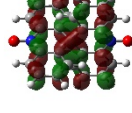
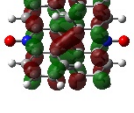
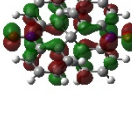
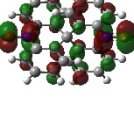
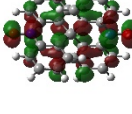
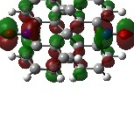
Table S9. The energy levels and $\langle S^2 \rangle$ in the triplet and singlet spin states for **SBDO-Si**.

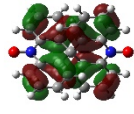
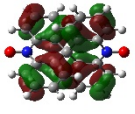
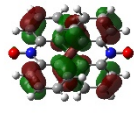
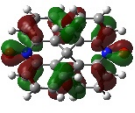
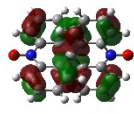
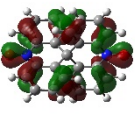
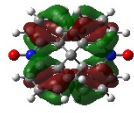
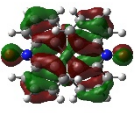
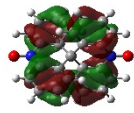
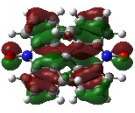
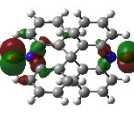
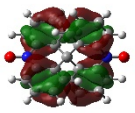
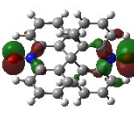
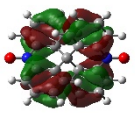
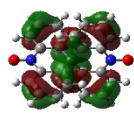
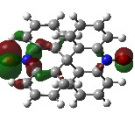
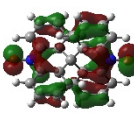
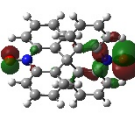
Spin states	E / au	$\langle S^2 \rangle$
$S = 1$ (triplet)	-1473.91657999	2.0006
$S = 0$ (singlet)	-1473.91652825	0.2272

Table S10. The energy levels and $\langle S^2 \rangle$ in the triplet and singlet spin states for **SBDO-Ge**.

Spin states	E / au	$\langle S^2 \rangle$
$S = 1$ (triplet)	-3261.37899748	2.0006
$S = 0$ (singlet)	-3261.37893832	0.2277

Table S11. Selected molecular orbitals of the triplet state ($S = 1$) and α and β spins for **SBDO-C** (isovalue = 0.03). Red and blue filled cells represent the occupied and unoccupied MOs, respectively.

MOs (α spin)	E / eV		MOs (β spin)	E / eV	
105	-0.492		105	-0.331	
104	-0.675		104	-0.579	
103	-0.834		103	-0.742	
102	-1.187		102	-1.070	
101	-1.187		101	-1.070	
100	-1.493		100	-1.419	
99 (SOMO)	-5.499		99	-3.020	
98 (SOMO)	-5.499		98	-3.020	

97	-6.940		97	-6.857	
96	-7.342		96	-7.178	
95	-7.342		95	-7.178	
94	-7.566		94	-7.307	
93	-7.616		93	-7.307	
92	-7.868		92	-7.467	
91	-7.868		91	-7.522	
90	-8.110		90	-7.589	
89	-8.191		89	-7.589	

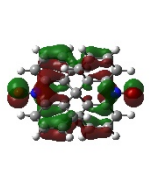
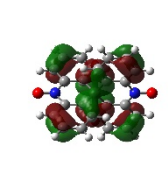
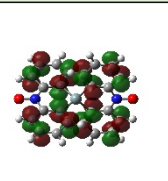
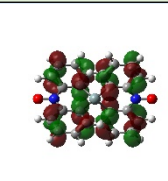
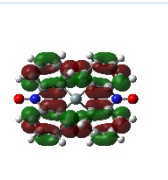
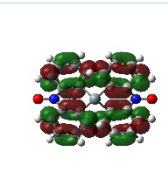
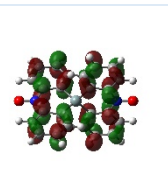
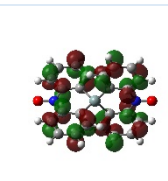
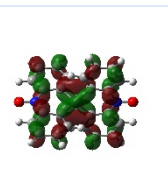
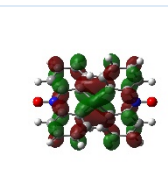
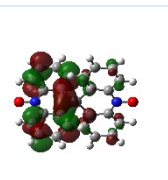
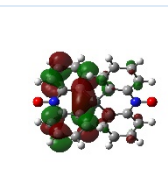
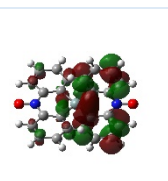
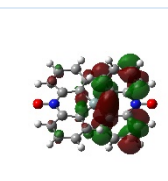
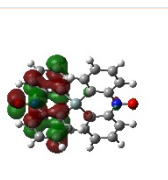
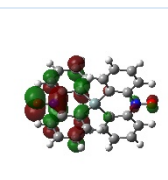
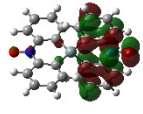
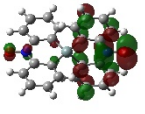
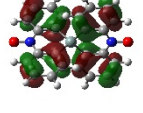
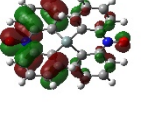
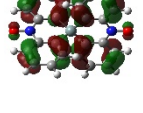
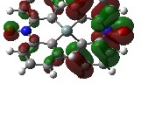
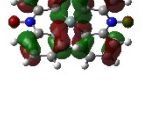
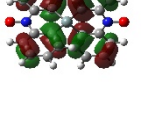
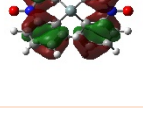
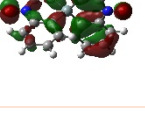
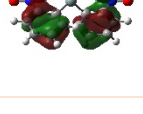
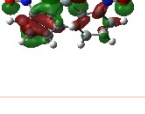
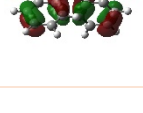
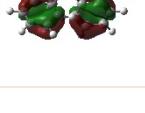
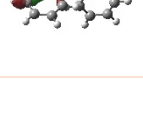

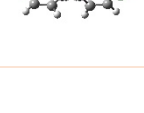
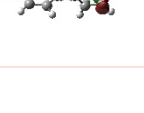
88	-8.191		88	-7.987	
----	--------	---	----	--------	---

Table S12. Selected molecular orbitals of the triplet state ($S = 1$) and α and β spins for SBDO-Si (isovalue = 0.03). Red and blue filled cells represent the occupied and unoccupied MOs, respectively.

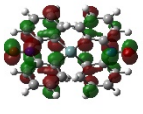
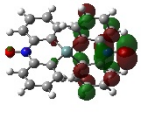
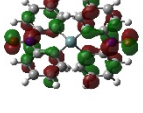
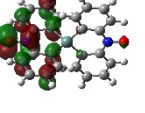
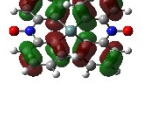
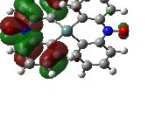
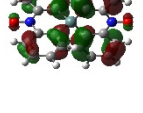
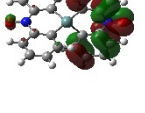
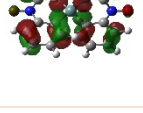
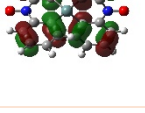
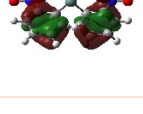
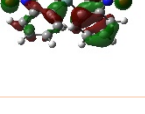

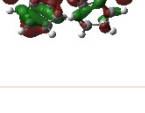


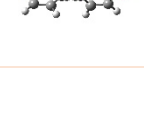
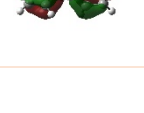
MOs (α spin)	E / eV		MOs (β spin)	E / eV	
109	-0.725		109	-0.630	
108	-0.729		108	-0.643	
107	-0.783		107	-0.670	
106	-1.429		106	-1.350	
105	-1.438		105	-1.382	
104	-1.438		104	-1.382	
103 (SOMO)	-5.617		103	-3.091	

102 (SOMO)	-5.617		102	-3.091	
101	-7.187		101	-7.097	
100	-7.400		100	-7.097	
99	-7.400		99	-7.109	
98	-7.553		98	-7.401	
97	-7.557		97	-7.401	
96	-7.751		96	-7.470	
95	-7.833		95	-7.475	
94	-7.833		94	-7.574	

93	-8.154		93	-7.574	
92	-8.154		92	-7.655	

Table S13. Selected molecular orbitals of the triplet state ($S = 1$) and α and β spins for **SBDO-Ge** (isovalue = 0.03). Red and blue filled cells represent the occupied and unoccupied MOs, respectively.

MOs (α spin)	E / eV		MOs (β spin)	E / eV	
118	-0.721		118	-0.023	
117	-0.735		117	-0.024	
116	-0.835		116	-0.026	
115	-1.326		115	-0.046	
114	-1.336		114	-0.047	
113	-1.336		113	-0.047	

112 (SOMO)	-5.605		112	-0.113	
111 (SOMO)	-5.605		111	-0.113	
110	-7.266		110	-0.261	
109	-7.353		109	-0.261	
108	-7.353		108	-0.264	
107	-7.563		107	-0.269	
106	-7.569		106	-0.269	
105	-7.696		105	-0.275	
104	-7.817		104	-0.275	

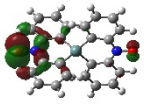
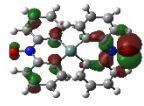
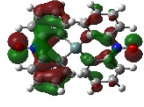
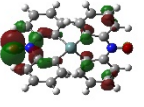
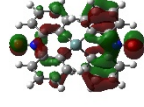
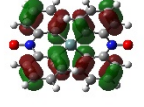
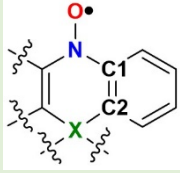
103	-7.817		103	-0.278	
102	-8.117		102	-0.278	
101	-8.117		101	-0.279	

Table S14. Spin densities for **SBDO-C**, **SBDO-Si** and **SBDO-Ge**.

	SBDO-C	SBDO-Si	SBDO-Ge
O	+0.450	+0.474	+0.436
N	+0.362	+0.351	+0.344
C1	-0.118	-0.119	-0.129
C2	+0.149	+0.152	+0.203
X	-0.054	-0.030	-0.070

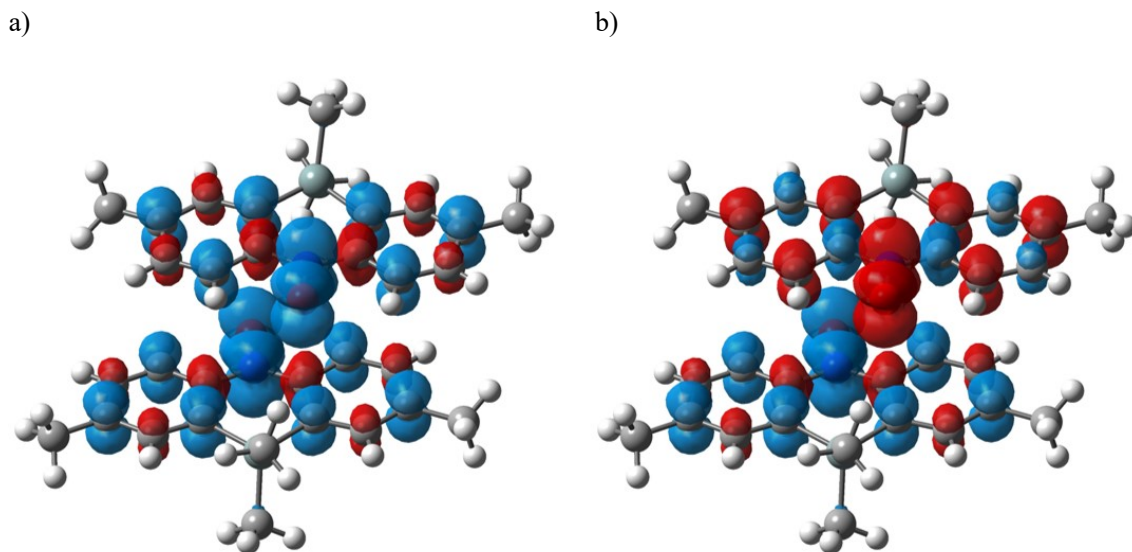


Fig. S11. Spin density maps drawn from the DFT MO calculations accompanied with the intermolecular contacts (N2 \cdots C41 and N3 \cdots C21) in **1-Si** in the (a) triplet and (b) singlet states. The geometrical parameters are from the crystallographic results. Blue and red lobes stand for positive and negative spin densities, respectively, with the isocontour of 0.002 e \AA^{-3} .

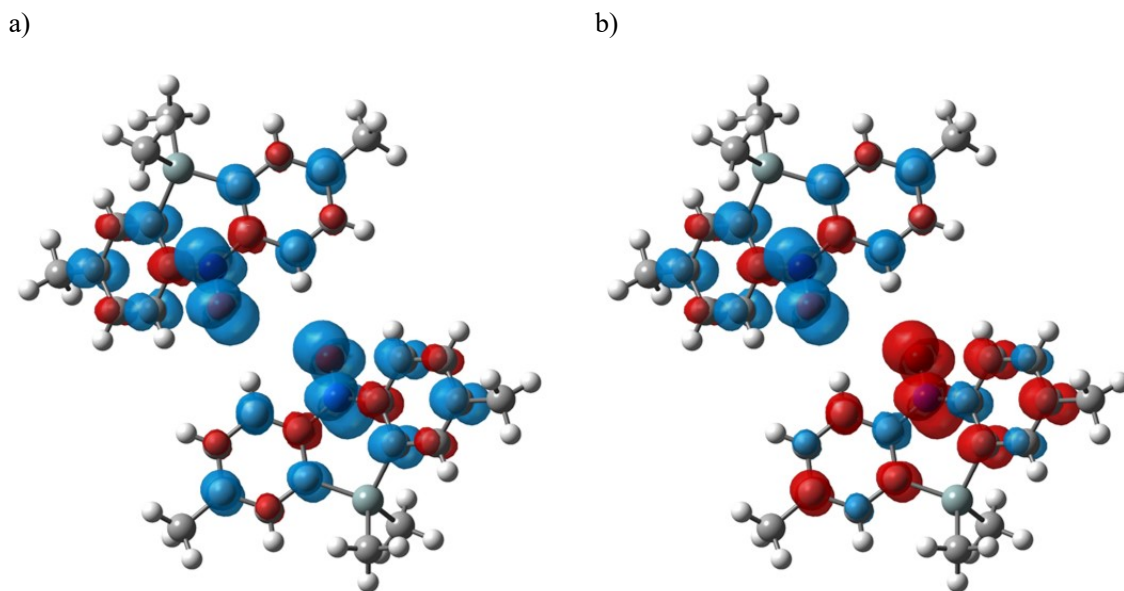


Fig. 12. Spin density maps drawn from the DFT MO calculations accompanied with the intermolecular contact (O1 \cdots O4) in **1-Si** in the (a) triplet and (b) singlet states. The geometrical parameters are from the crystallographic results. Blue and red lobes stand for positive and negative spin densities, respectively, with the isocontour of 0.002 e \AA^{-3} .

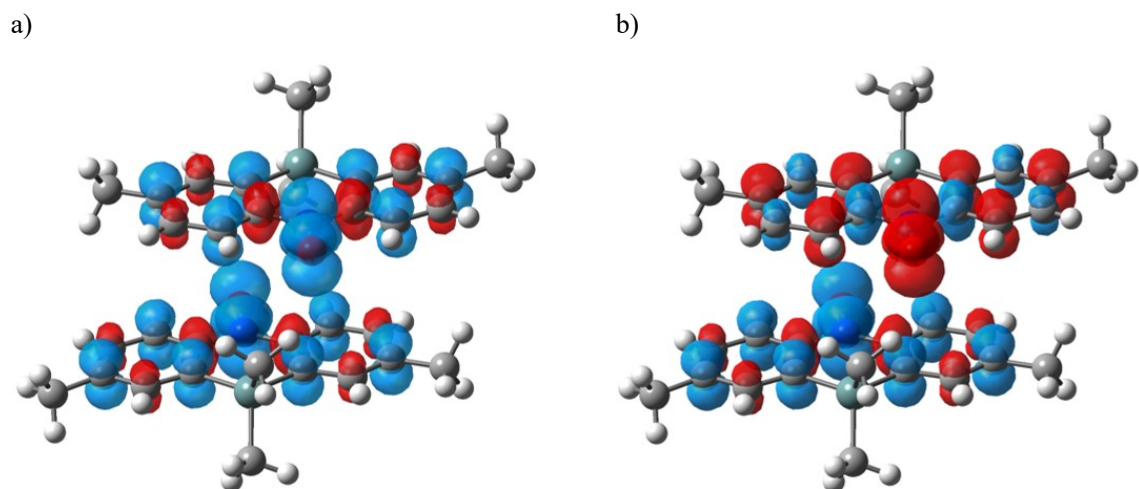


Fig. S13. Spin density maps drawn from the DFT MO calculations accompanied with the intermolecular contacts (O2···C21 and N2···C22) in **1-Ge** in the (a) triplet and (b) singlet states. The geometrical parameters are from the crystallographic results. Blue and red lobes stand for positive and negative spin densities, respectively, with the isocontour of $0.002 \text{ e } \text{\AA}^{-3}$.

Magnetic measurements

The direct current magnetic susceptibilities of **1-Si** and **1-Ge** were measured on a Quantum Design MPMS-XL7AC SQUID magnetometer equipped with a 7 T coil in a temperature range of 2–300 K under the static field of 0.5 T. The magnetic data were corrected using diamagnetic blank data of the sample holder measured. The diamagnetic contribution of the sample itself was estimated from Pascal's constants.^{S6}

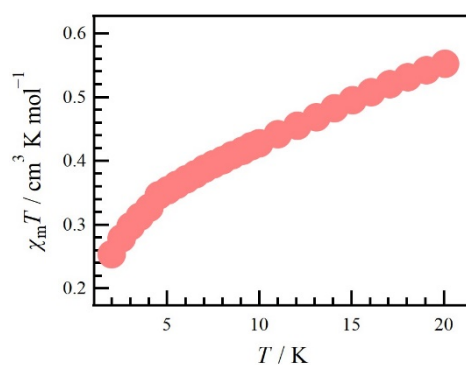


Fig. S14. Temperature dependence of the product $\chi_m T$ for **1-Si** in the temperature range of 2–20 K.

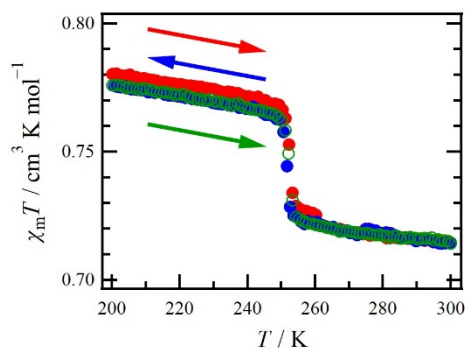


Fig. S15. Temperature dependence of the product $\chi_m T$ for **1-Ge**, The red, blue and green colours represent the 1st heating, 1st cooling and 2nd heating processes, respectively.

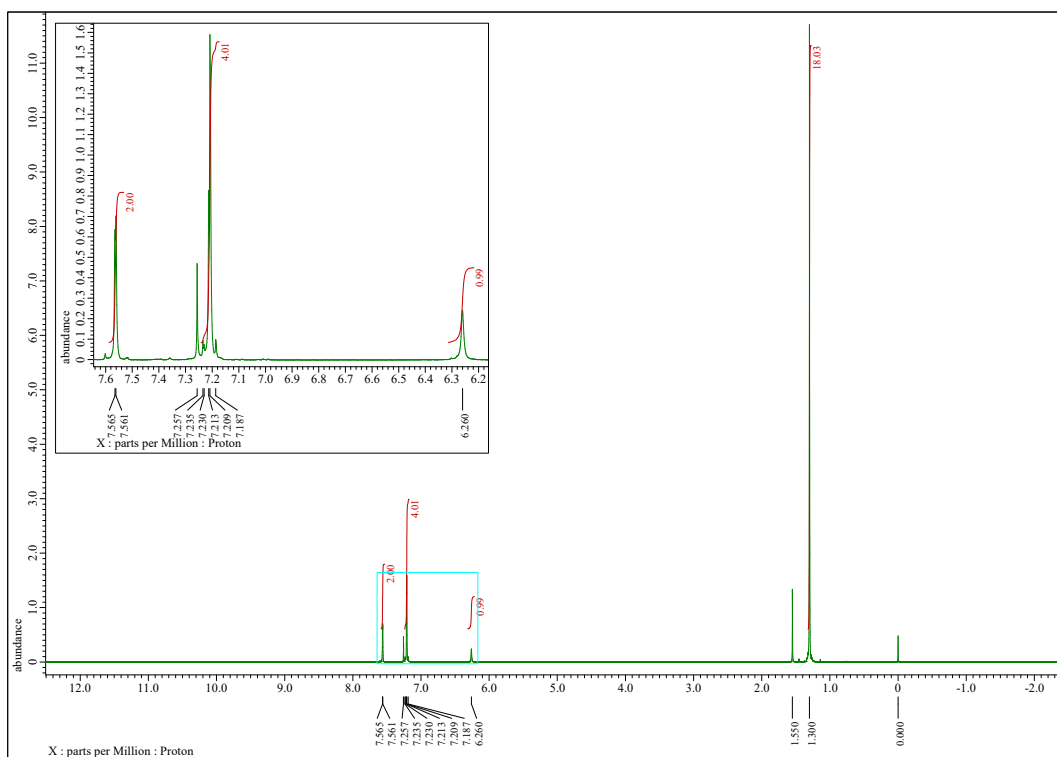


Fig. S16. ^1H NMR spectrum for **2**.

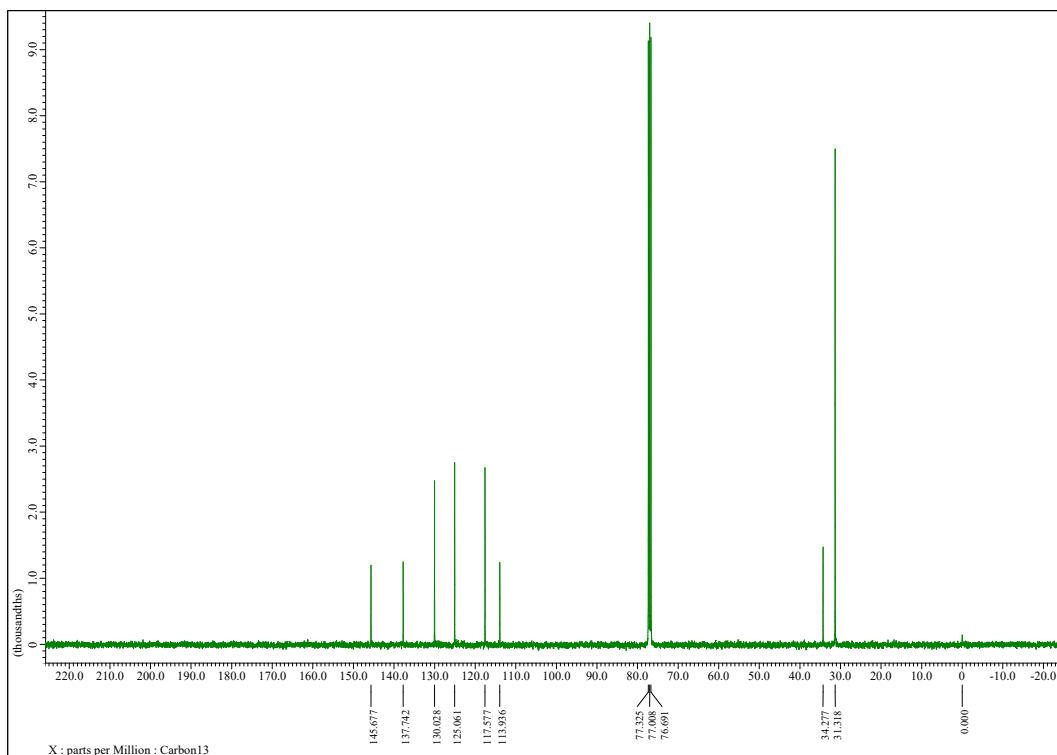


Fig. S17. ^{13}C NMR spectrum for **2**.

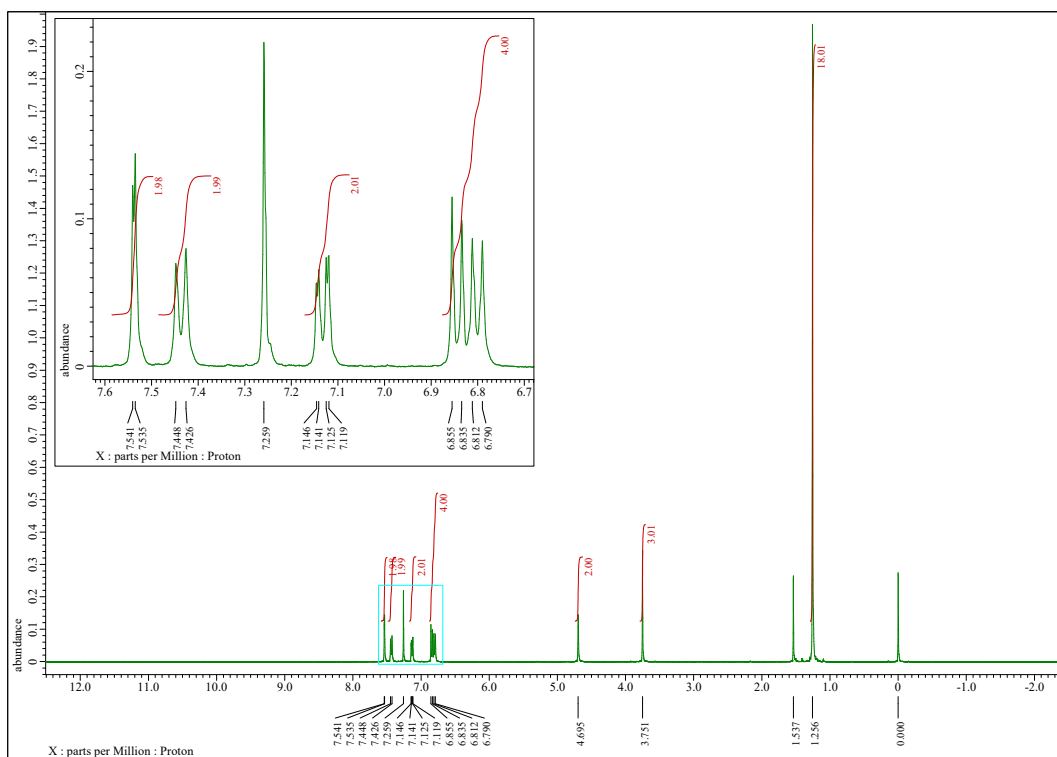


Fig. S18. ¹H NMR spectrum for **3**.

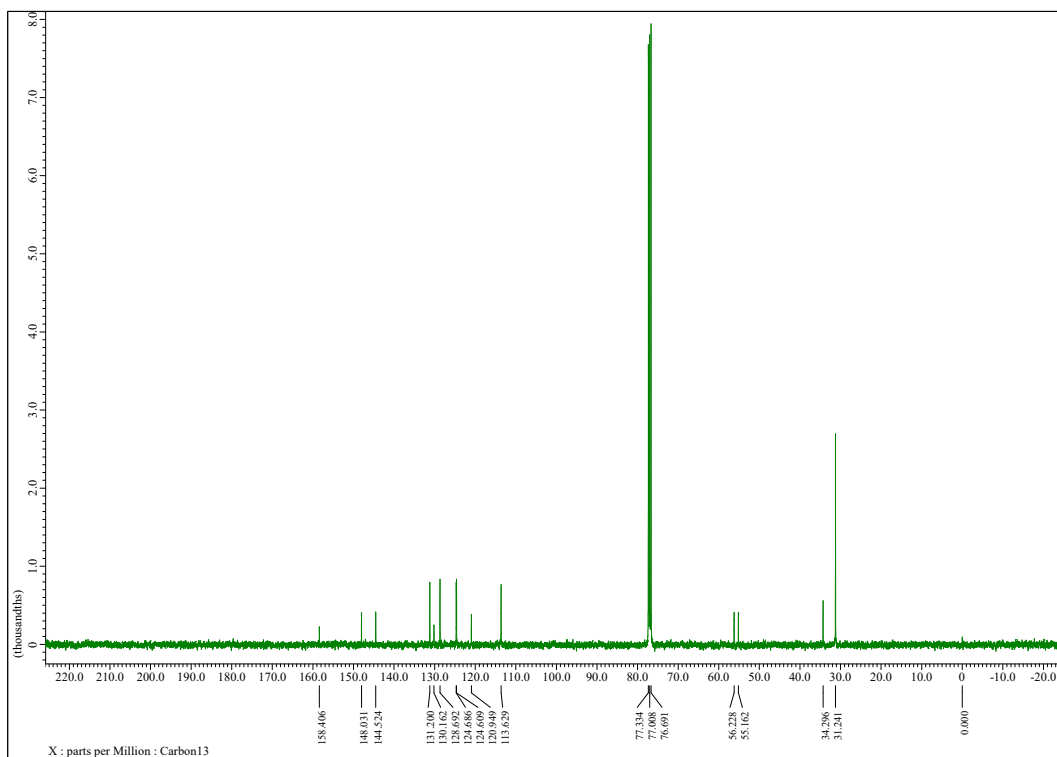


Fig. S19. ¹³C NMR spectrum for **3**.

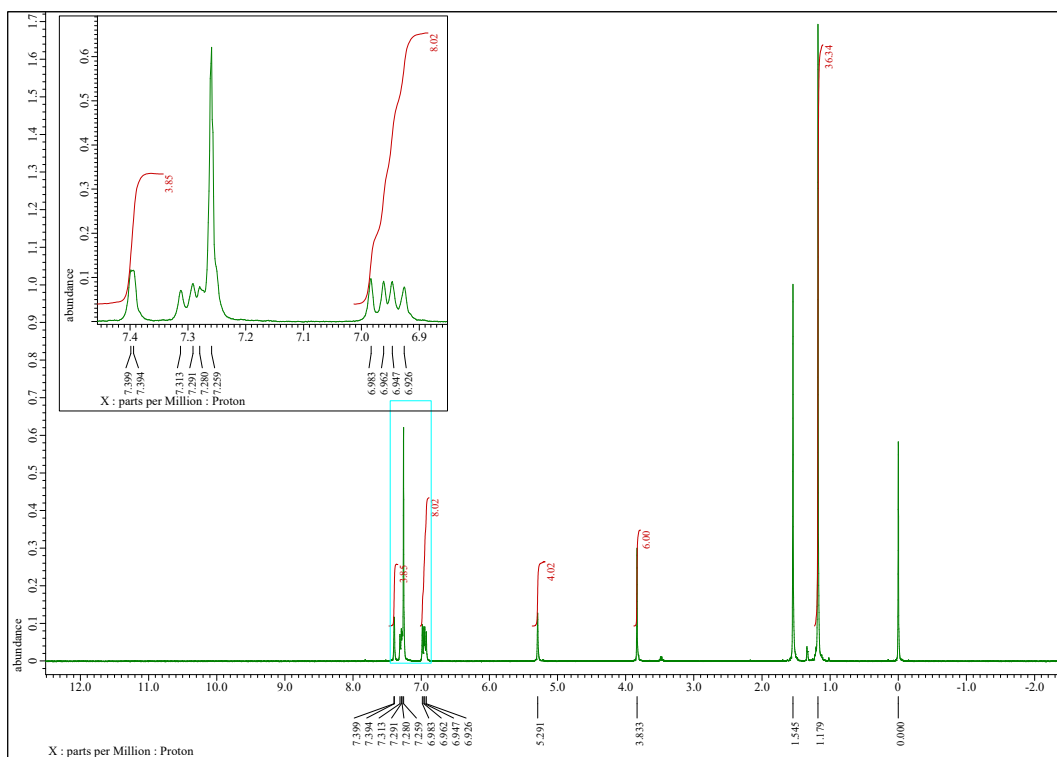


Fig. S20. ¹H NMR spectrum for 4-Si.

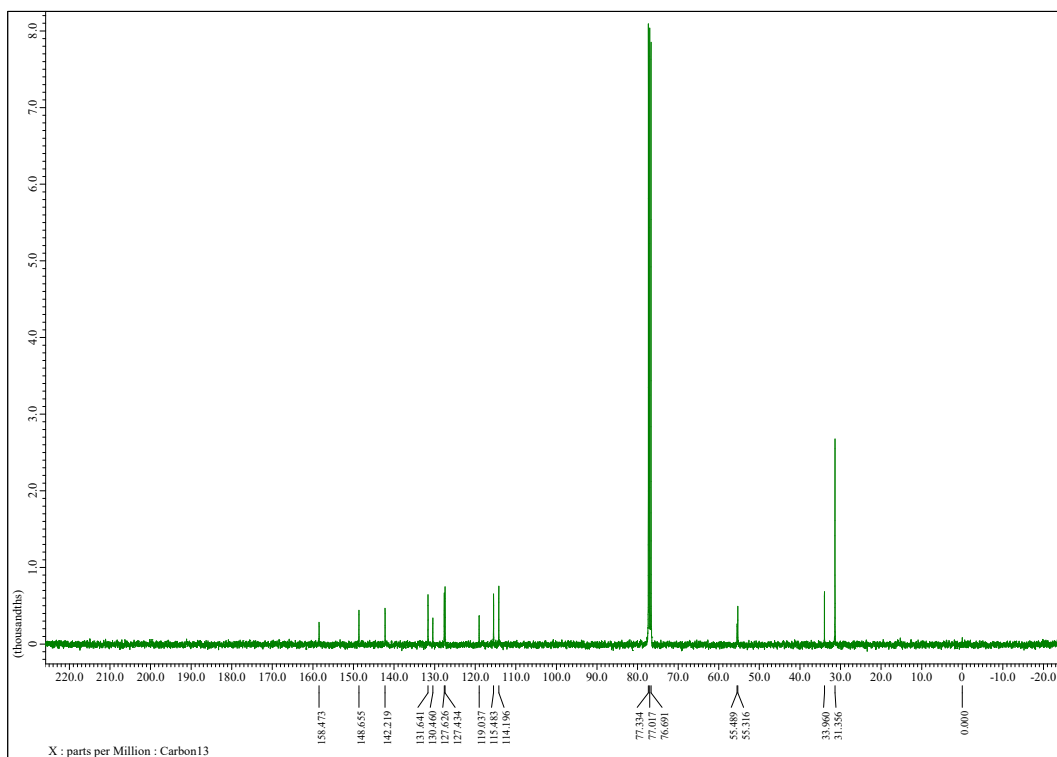


Fig. S21. ¹³C NMR spectrum for 4-Si.

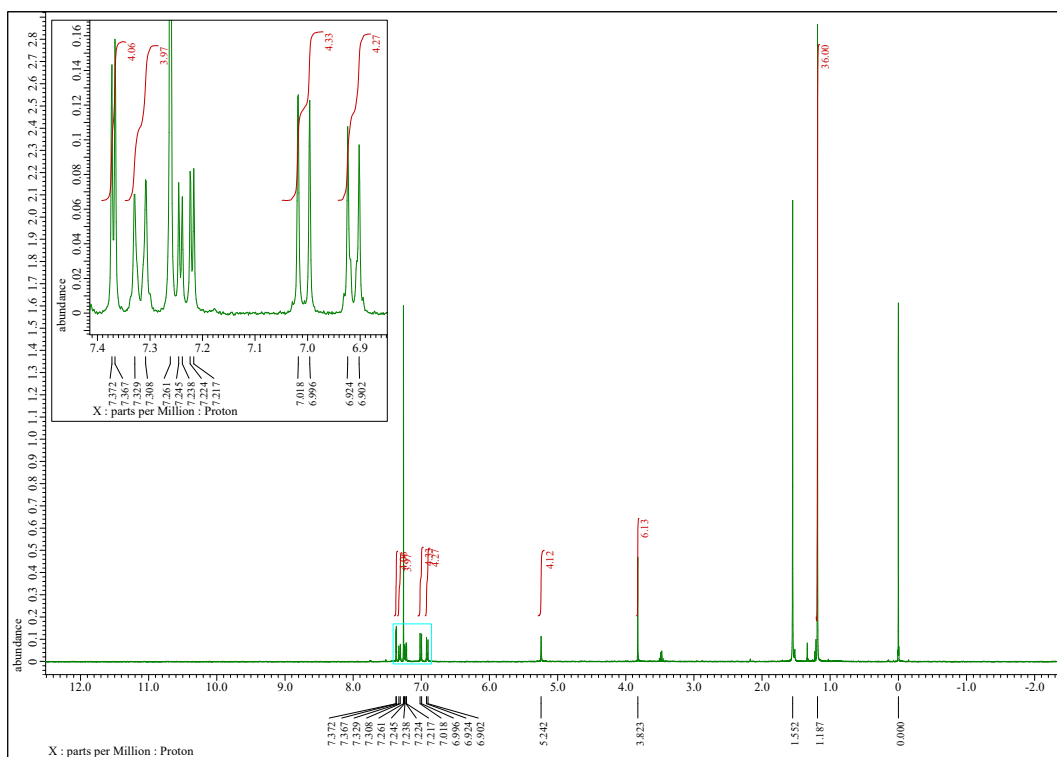


Fig. S22. ¹H NMR spectrum for 4-Ge.

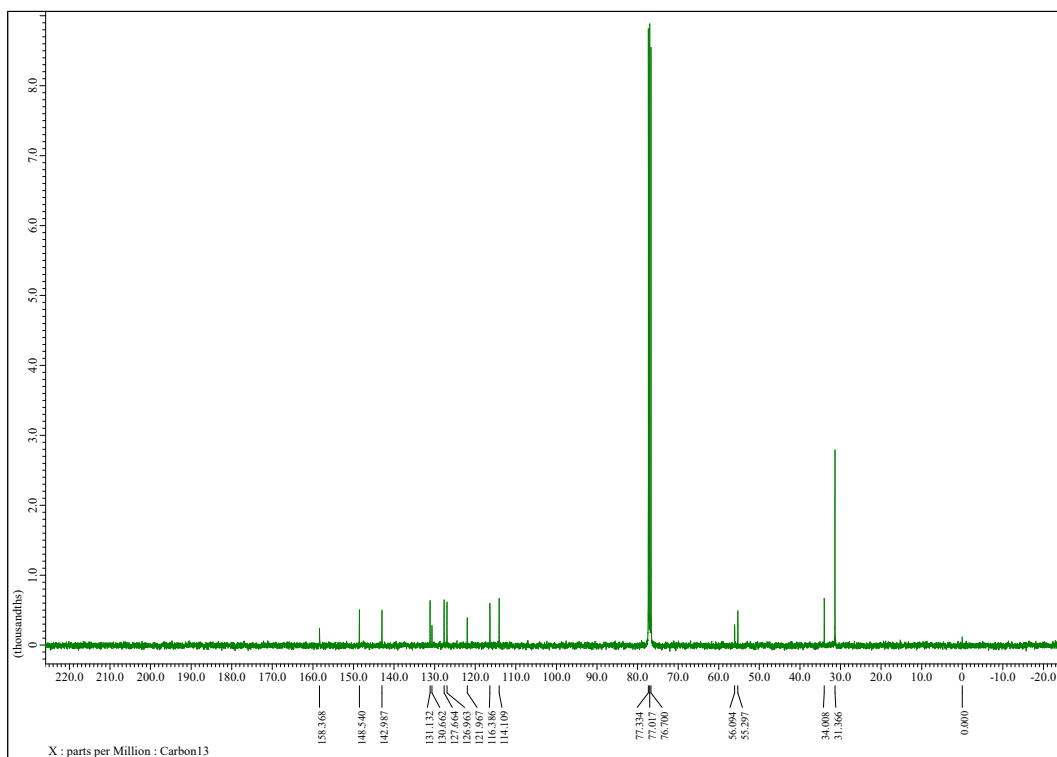


Fig. S23. ¹³C NMR spectrum for 4-Ge.

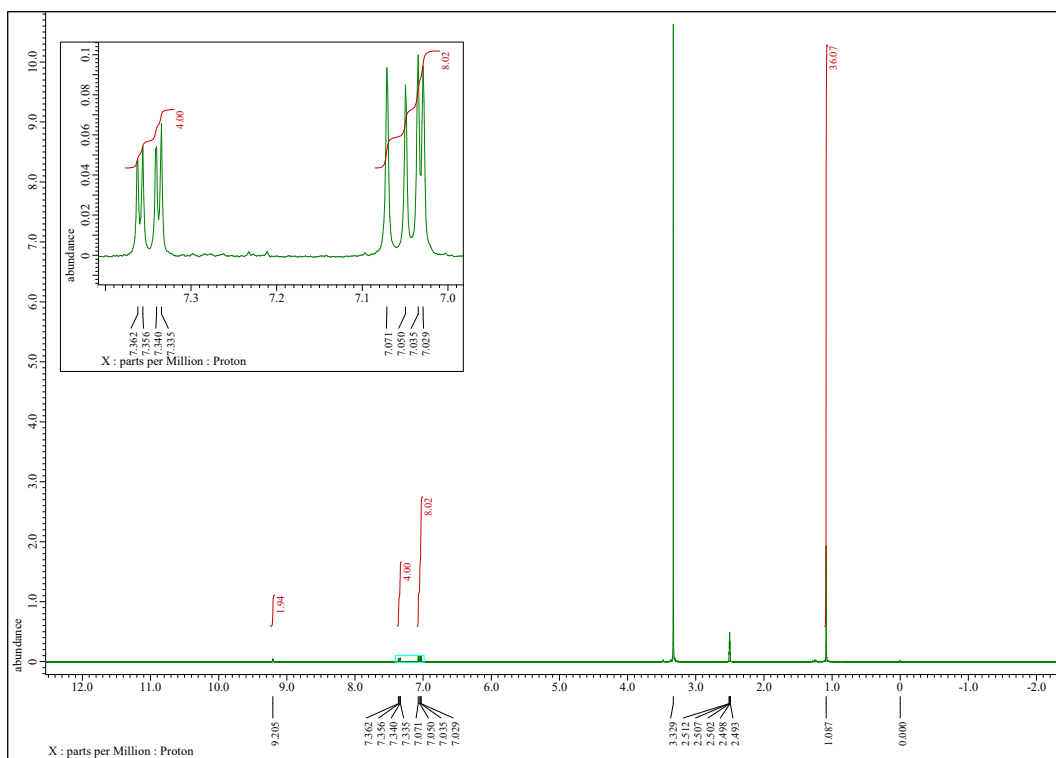


Fig. S24. ^1H NMR spectrum for 5-Si.

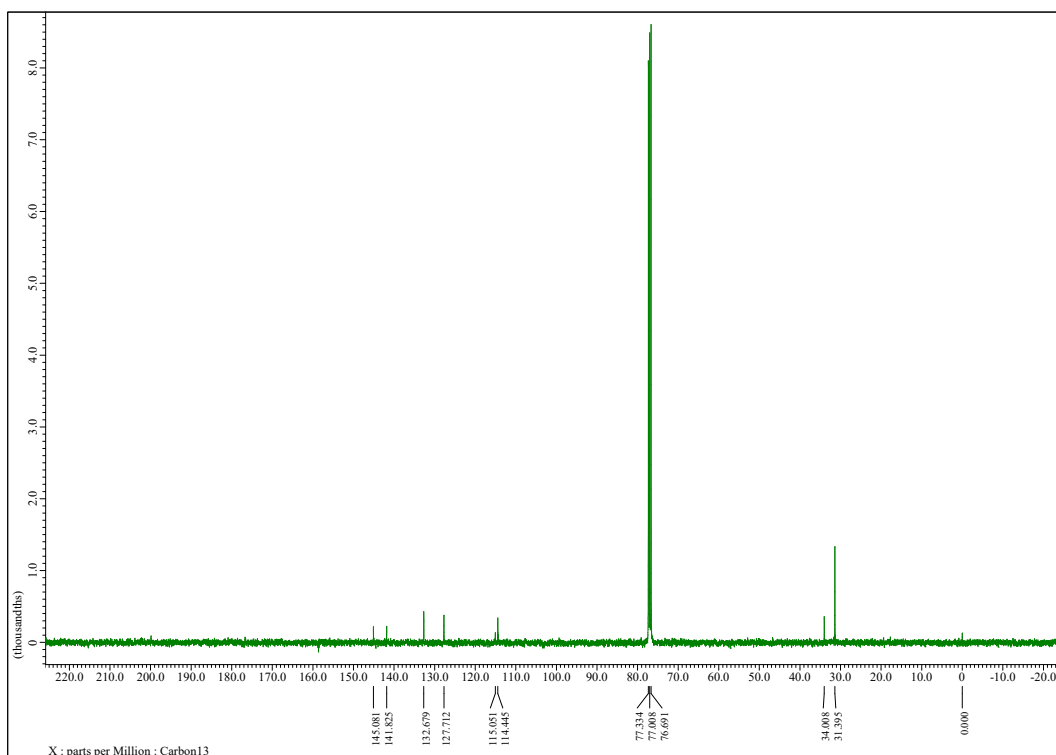


Fig. S25. ^{13}C NMR spectrum for 5-Si.

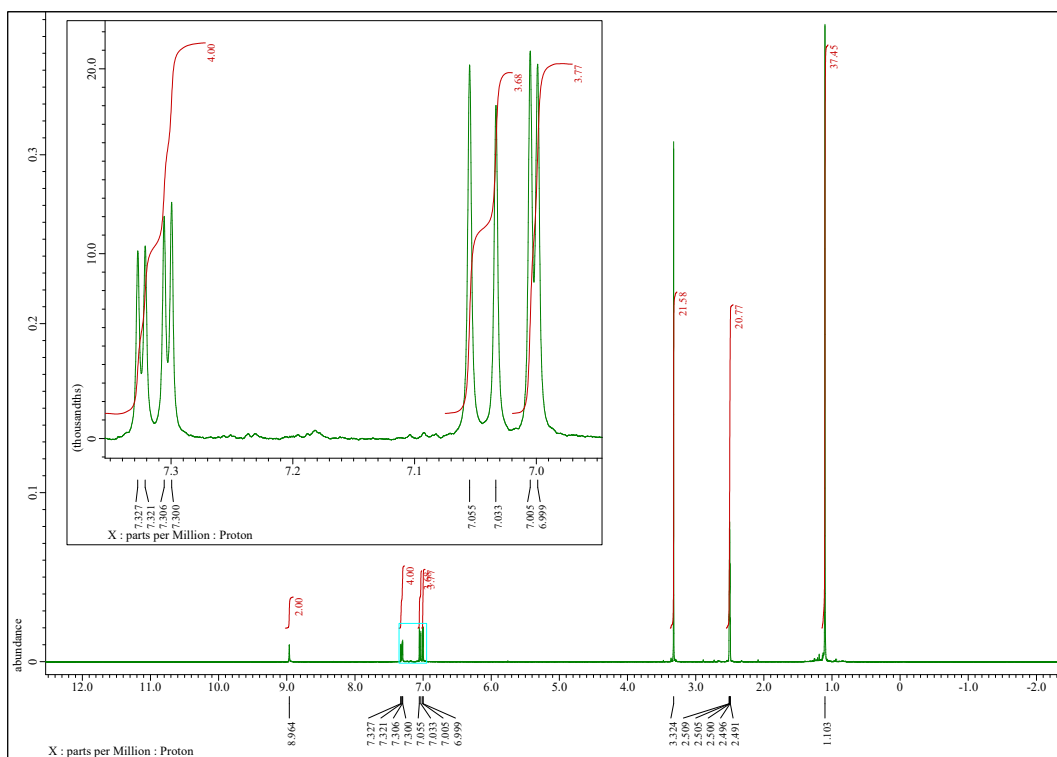


Fig. S26. ¹H NMR spectrum for **5-Ge**.

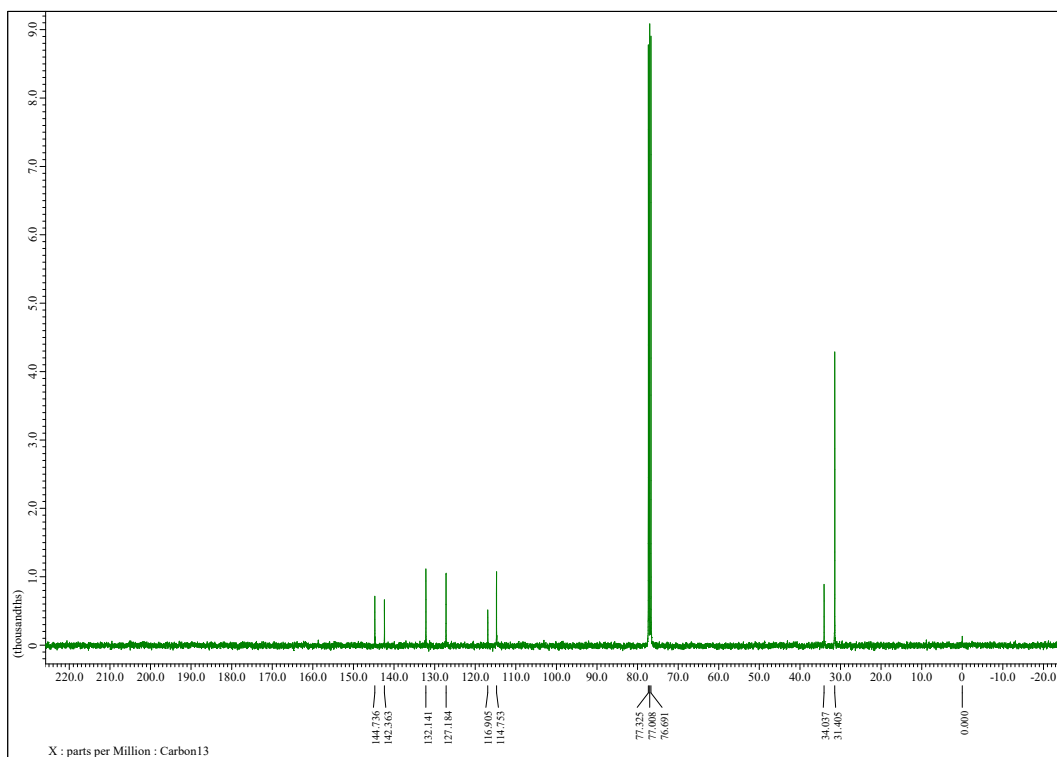


Fig. S27. ¹³C NMR spectrum for **5-Ge**.

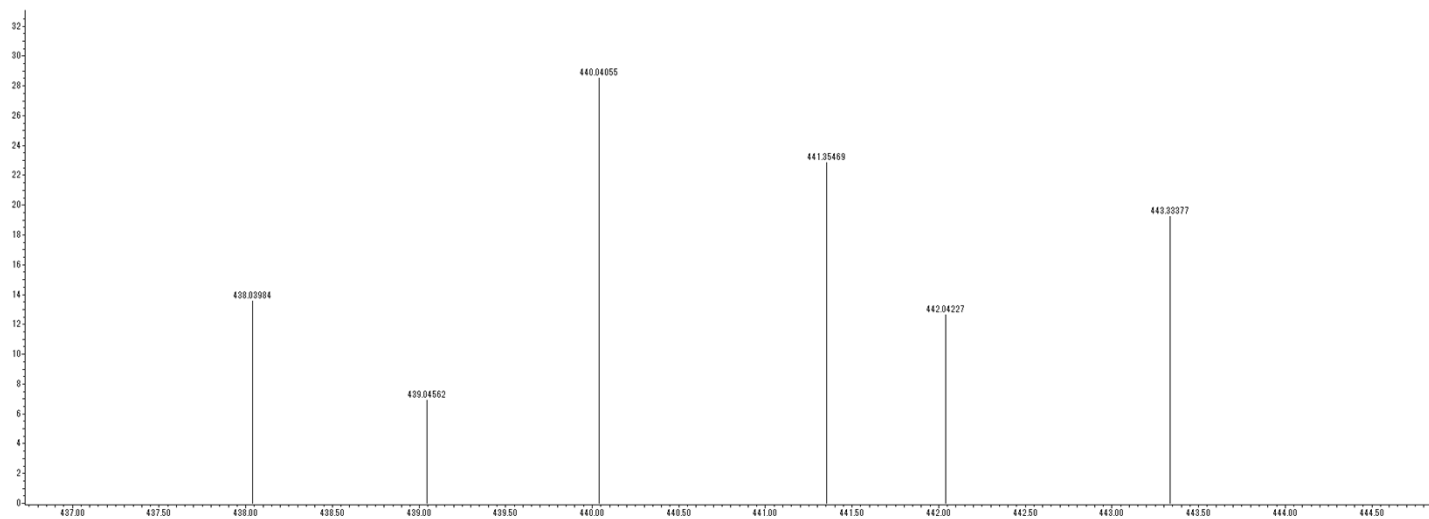


Fig. S28. HRMS spectrum of 2.

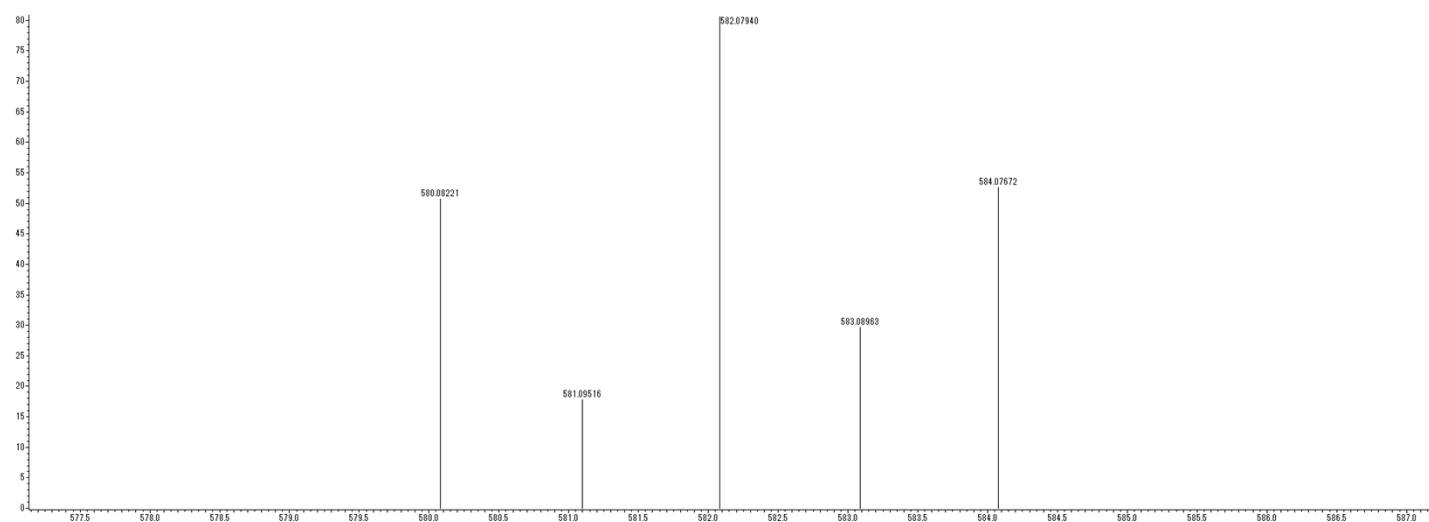


Fig. S29. HRMS spectrum of 3.

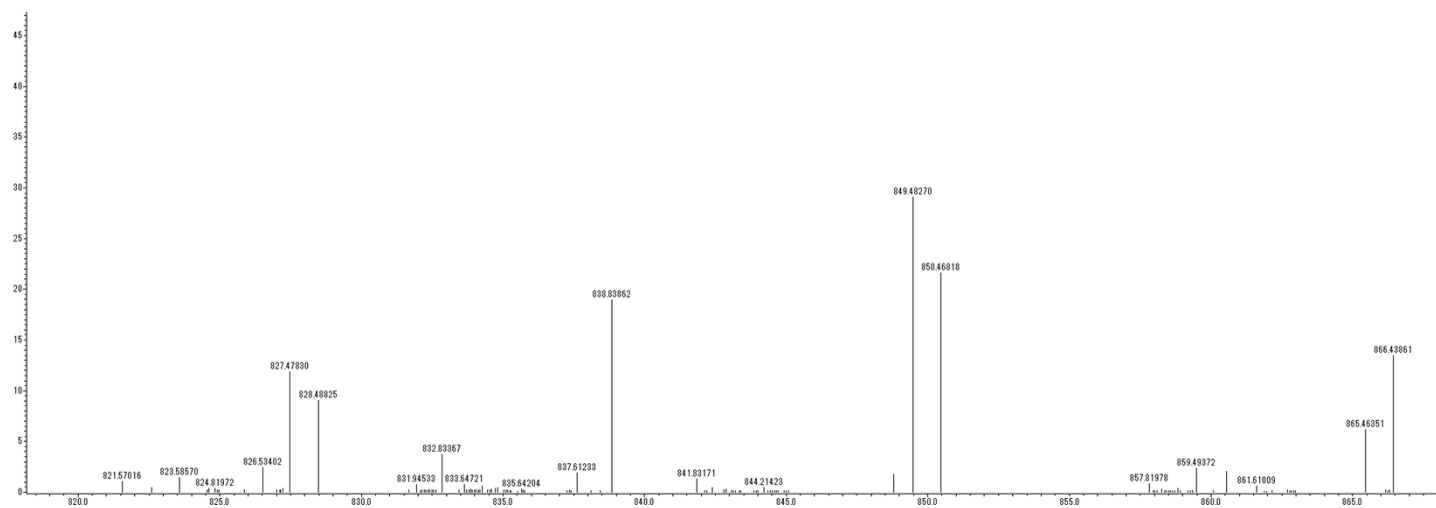


Fig. S30. HRMS spectrum of 4-Si.

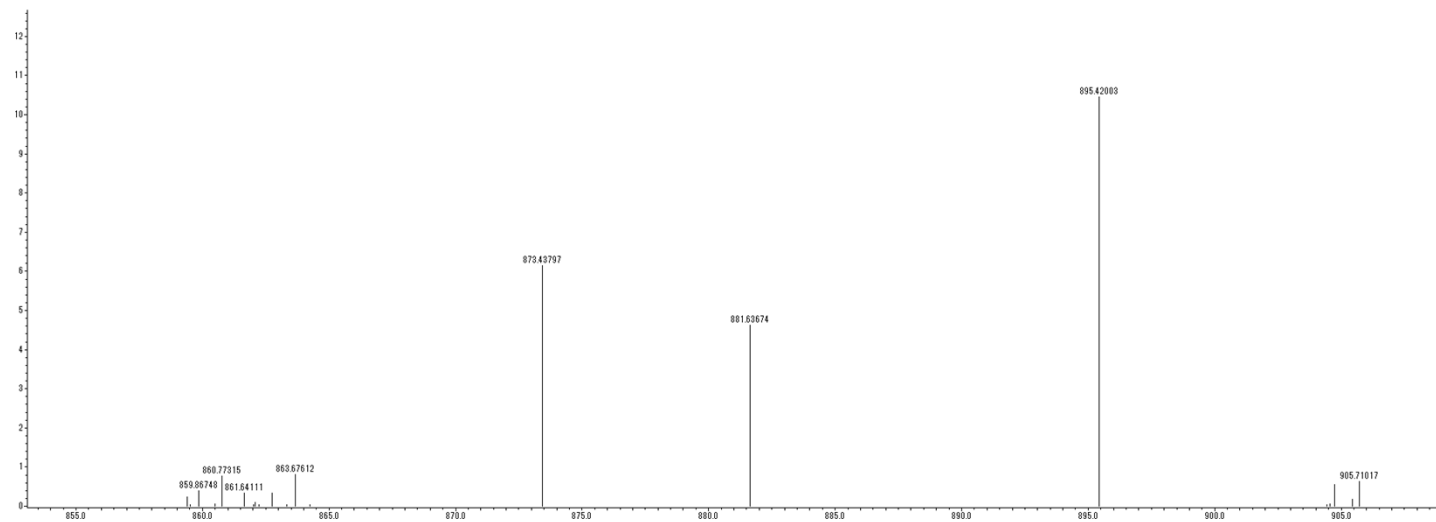


Fig. S31. HRMS spectrum of 4-Ge.

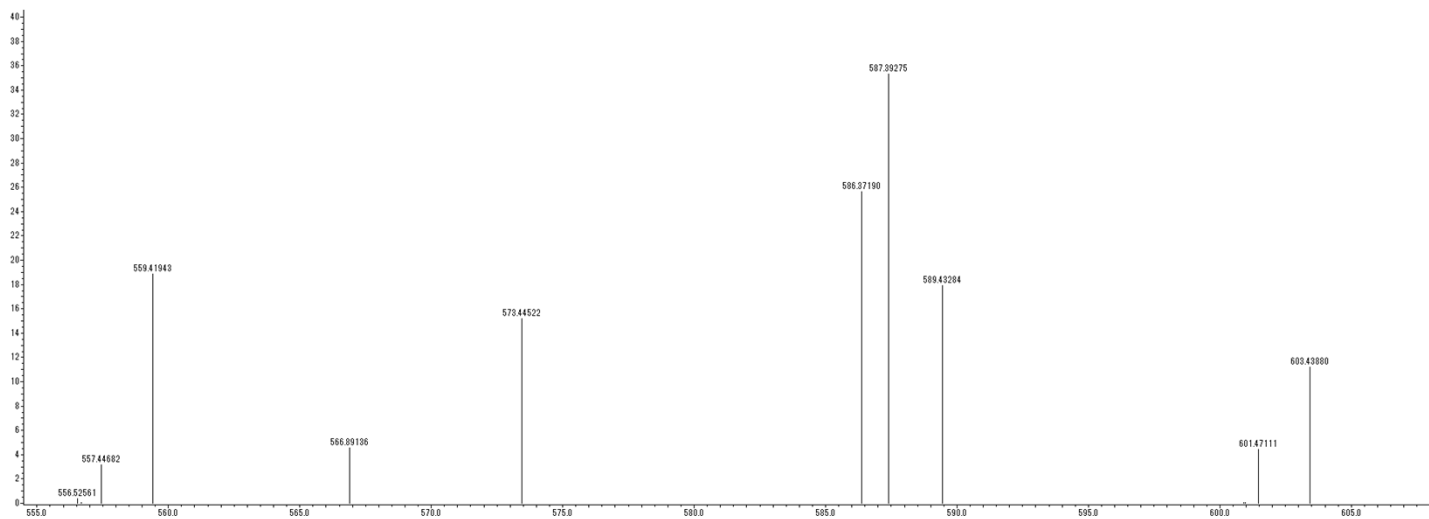


Fig. S32. HRMS spectrum of 5-Si.

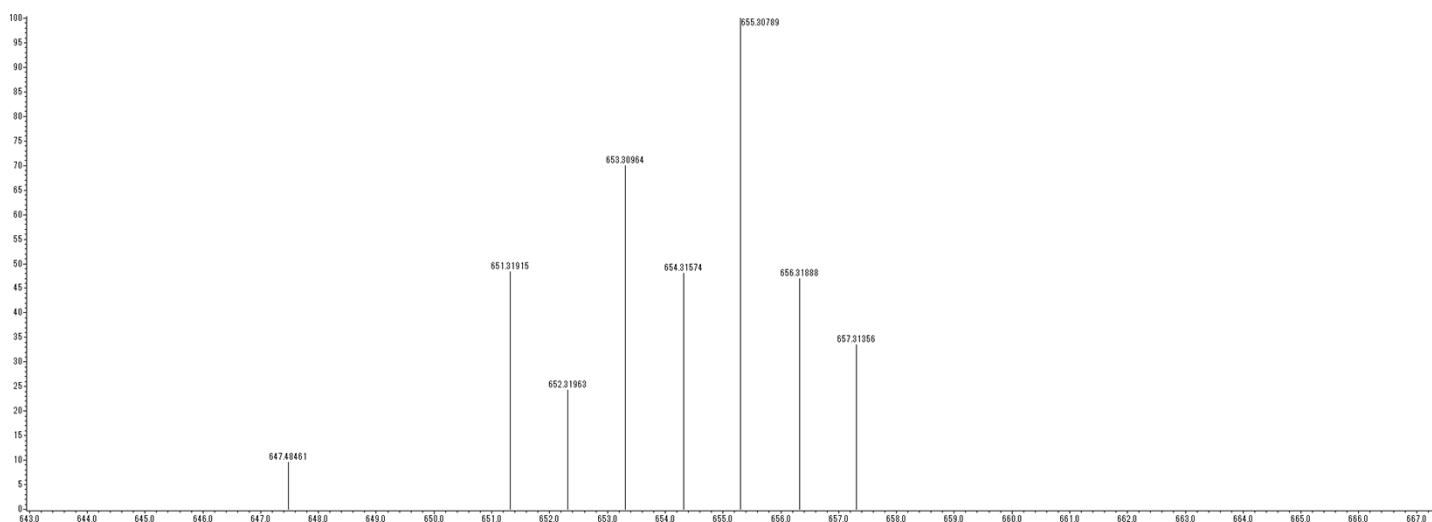


Fig. S33. HRMS spectrum of 5-Ge.

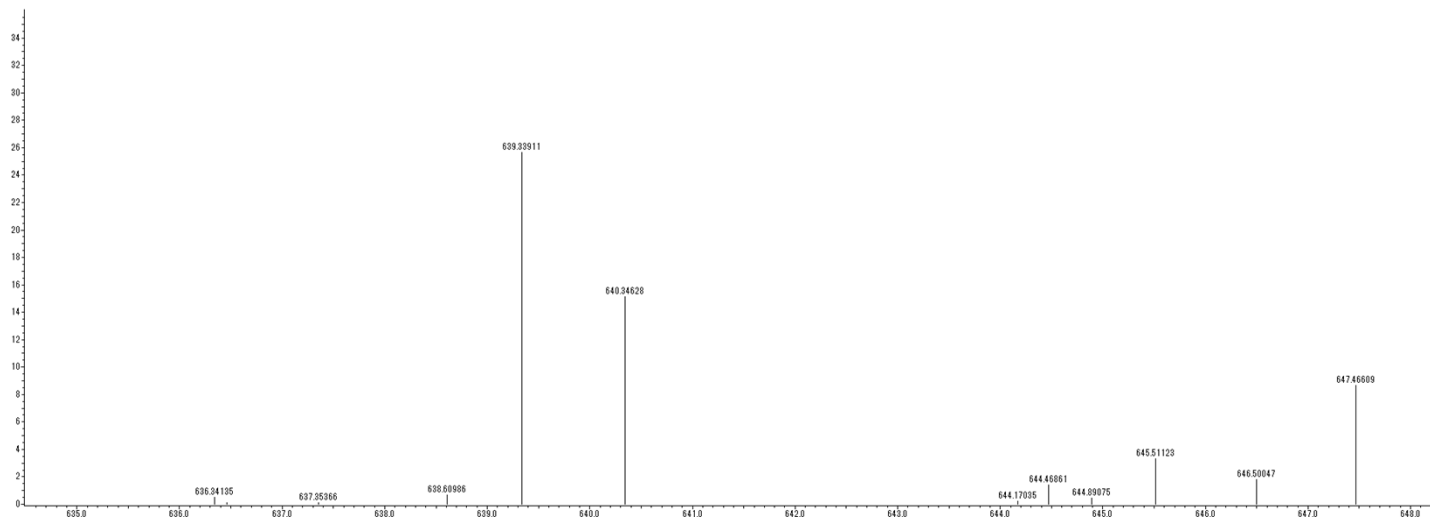


Fig. S34. HRMS spectrum of 1-Si.

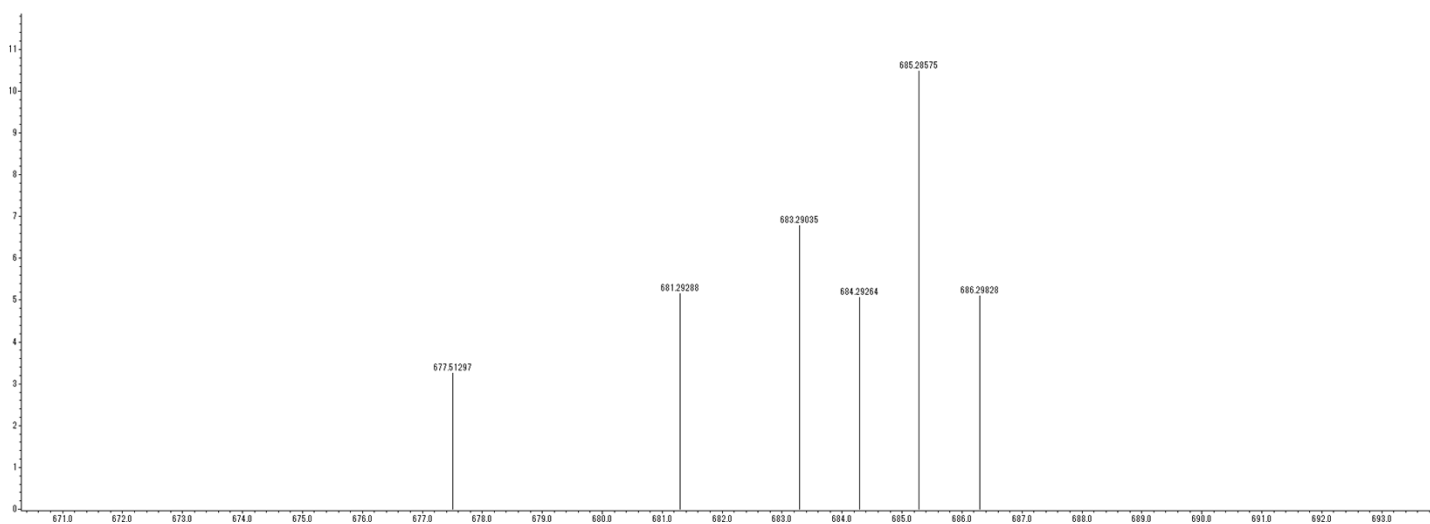


Fig. S35. HRMS spectrum of 1-Ge.

References

- S1. G. M. Sheldrick, SHELXT – Integrated space-group and crystal structure determination, *Acta Cryst.*, 2015, **A71**, 3–8.
- S2. G. M. Sheldrick, Crystal structure refinement with SHELXL, *Acta Cryst.*, 2015, **C71**, 3–8.
- S3. L. J. Bourhis, O. V. Dolomanov, R. J. Gildea, J. A. K. Howard and H. Puschmann, The anatomy of a comprehensive constrained, restrained refinement program for the modern computing environment – *Olex2* dissected, *Acta Cryst.*, 2015, **A71**, 59–75.
- S4. T. Kanetomo, K. Ichihashi, M. Enomoto and T. Ishida, Ground Triplet Spirobiradical: 2,2',7,7'-Tetra(*tert*-butyl)-9,9'(10*H*,10'*H*)-spirobiacridine-10,10'-dioxyl, *Org. Lett.*, 2019, **21**, 3909–3912.
- S5. M. J. Frisch, G. W. Trucks, H. B. Schlegel, G. E. Scuseria, M. A. Robb, J. R. Cheeseman, G. Scalmani, V. Barone, B. Mennucci, G. A. Petersson, H. Nakatsuji, M. Caricato, X. Li, H. P. Hratchian, A. F. Izmaylov, J. Bloino, G. Zheng, J. L. Sonnenberg, M. Hada, M. Ehara, K. Toyota, R. Fukuda, J. Hasegawa, M. Ishida, T. Nakajima, Y. Honda, O. Kitao, H. Nakai, T. Vreven, J. A. Montgomery Jr., J. E. Peralta, F. Ogliaro, M. Bearpark, J. J. Heyd, E. Brothers, K. N. Kudin, V. N. Staroverov, R. Kobayashi, J. Normand, K. Raghavachari, A. Rendell, J. C. Burant, S. S. Iyengar, S. S. J. Tomasi, M. Cossi, N. Rega, J. M. Millam, M. Klene, J. E. Knox, J. B. Cross, V. Bakken, C. Adamo, J. Jaramillo, R. Gomperts, R. E. Stratmann, O. Yazyev, A. J. Austin, R. Cammi, C. Pomelli, J. W. Ochterski, R. L. Martin, K. Morokuma, V. G. Zakrzewski, G. A. Voth, P. Salvador, J. J. Dannenberg, S. Dapprich, A. D. Daniels, O. Farkas, J. B. Foresman, J. V. Ortiz, J. Cioslowski, and D. J. Fox, Gaussian09, Revision A.02; Gaussian, Inc.: Wallingford, CT, 2009.
- S6. O. Kahn, *Molecular Magnetism*, VCH-Verlag, Weinheim, New York, 1993.